Electrocatalytic Application of Ni/Fe MOF for Methanol Oxidation in DMFC

By

Muhammad Mohtashim

School of Chemical and Materials Engineering

National University of Science and Technology

2021

Electrocatalytic Application of Ni/Fe MOF for Methanol Oxidation in DMFC

Name: Muhammad Mohtashim

Registration No: 00000277500

This thesis is submitted as a partial fulfillment of the requirements for the degree of

MS in Chemical Engineering

Supervisor Name: Dr. Tayyaba Noor

School of Chemical and Materials Engineering (SCME)

National University of Science and Technology (NUST)

H-12, Islamabad, Pakistan

January, 2021

Dedication

By the grace of Almighty Allah, who is the most Beneficent and the most merciful

This research is dedicated to my parents, who have always been my source of guidance and support.

To my supervisor who shared her knowledge, gave advice and encouraged me to fulfill my tasks.

And to all my fellows, with whom I worked with and shared good memories.

Acknowledgements

There is no one except Almighty Allah, whose will is necessary for everything and anything in this world, who favored us with the capacity to think and made us anxious to investigate this entire universe. Infinite greetings upon the Holy Prophet Muhammad (PBUH), the reason for the creation of the universe and wellspring of information and blessing for whole humankind.

I pay my sincere gratitude to Dean and Principle of SCME, Prof. Dr. Amir Azam Khan for being a source of great inspiration and for facilitation of this research work. I am indebted to HOD Chemical Engineering Dr. Muhammad Bilal Khan Niazi for facilitating me throughout my course at NUST.

From the core of my heart, I am thankful to my research supervisor, Dr. Tayyaba Noor for her unwavering technical and moral support and enlightening me with a research vision and pushing me for excellence. Her quest for perfection and excellence had been a source of inspiration and driving force. It is her consistent and encouragement that empowered me to achieve the onerous milestone.

I extend my sincere gratitude towards my guidance and committee members: Dr. Sarah Farrukh and Dr. Abdul Qadeer Malik for guiding and supporting me in my research course. It would not have been possible without them. I express my gratitude to onerous Mr. Muhammad Zeeshan, Mr. Malik Nouman Shahzad and Mr. Zafar for their significant contribution.

I am highly obligated to my family for their never-ending love. Thanks for believing in me, wanting the best for me and inspiring me to follow my passion. My friends, colleagues and well-wishers for your support, advice and encouragement, I thank you all.

Abstract

Fuel cells are the way towards green environment with its application reaching landmark where it can be employed on mass scales for consumer usage. Previously used catalyst such as Pt, Rh, Ru and Pd being expensive, faced the challenge of catalyst poisoning and slow reaction kinetics. The solution to these problems is an effective, low cost and efficient catalyst which can benefits the advantages of noble catalyst while suppressing the negatives faced by them.

This thesis presents the research on novel bimetallic Ni/Fe MOF as catalyst of methanol oxidation reaction in DMFC. The catalyst was synthesized using hydrothermal process. To enhance the characteristic of catalyst, reduced graphene oxide was incorporated in catalyst with 1-5 and 8 wt%. Reduced graphene oxide (rGO) was synthesized using modified hummers method. Incorporation of rGO in Ni/Fe MOF enhanced the catalytic activity and conductivity by increasing surface area. As for the trend of 1-5 wt%, the performance of catalyst increases, however 8 wt% showed less catalytic activity due to domination of rGO on active sites of catalyst which hindered the oxidation of methanol on Ni/Fe MOF. Characterization of samples was done by SEM, XRD and FTIR. XRD described the crystallinity of catalyst and reflected that rGO has no effect on crystallinity of catalyst. SEM revealed information about morphology of catalyst and FTIR confirmed the presence of functional group in catalyst. Electrochemical studies were carried out using CV, EIS and Chronoamperometry tests. With current density of 486.14 mA/cm^2, Ni/Fe MOF with 8 wt% rGO composite showed best catalytic activity at 50 mV/s scan rate. Chronoamperometry showed stability of 51% for the passage of an hour while EIS confirmed the lowest charge transfer resistance for 5 wt% rGO-Ni/Fe MOF.

Keywords: Reduced Graphene Oxide, Metal Organic Frameworks, Ni/Fe MOF, Hydrothermal process, modified hummers method, Electrocatalysis.

Table of Contents

Dedication i

Acknowledgements ii

Abstract iii

List of Figures vii

List of Acronyms ix

List of Tables x

Chapter 1 1

Introduction 1

1.1 Energy Demand 1

1.2 Fuel cell 1

1.2.1 Types of Fuel Cell 3

1.2.1.1 Phosphoric Acid Fuel Cell 3

1.2.1.3 Molten Carbonate Fuel Cell 4

1.2.1.4 Solid Oxide Fuel Cell 5

1.2.1.5 Proton Exchange Membrane Fuel Cell (PEMFC) 6

1.2.2 Membranes for PEMFC 7

1.2.3 Direct methanol fuel cell (DMFC) 9

1.2.3.1 Challenges associated with DMFC 9

1.3 Metal organic frameworks (MOF) 11

1.3.1 Synthesis of MOF 12

1.3.1.1 Microwave assisted technique 13

1.3.1.2 Electrochemical assisted technique 13

1.3.1.3 Mechano-chemical synthesis technique 13

1.3.1.4 Sonochemical synthesis 14

1.3.1.5 Slow evaporation technique 14

1.3.1.6 Solvothermal Method 15

1.3.2 Applications of MOFs 15

1.3.2.1 MOFs for gas separation and storage 15
1.3.2.3 MOFs for sensing 17
1.4 Characterization Techniques 17
1.4.1 X-ray diffraction: 17
1.4.2 Scanning electron microscope (SEM) 18
1.4.3 Fourier Transform Infrared Spectroscopy (FTIR) 19
1.4.4 Raman Spectroscopy 20
1.5 Catalyst for Methanol Oxidation Reaction 22
1.6 Research Objectives 23
Chapter 2 24
Literature Review 24
Chapter 3 29
Experimental Section 29
3.1 Synthesis of bimetallic Ni-Fe MOF 29
3.1.1 Materials 29
3.1.2 Equipment 29
3.1.3 Method of preparation 29
3.2 Synthesis of Graphene oxide 30
3.2.1 Materials 30
3.2.2 Equipment 30
3.2.3 Method of preparation 30
3.3 Synthesis of reduced graphene oxide (rGO) 32
3.3.1 Materials 33
3.4 Synthesis of rGO-Ni/Cu MOF composites 34
3.5 Preparation of modified working electrode 36
3.6 Electrochemical testing techniques 37
3.6.1 Cyclic voltammetry 37

3.6.2 Electrochemical Impedance Spectroscopy 39
3.6.3 Chronoamperometry 39

Chapter 4 41

4.1 Characterization Techniques 41
4.1.1 Scanning electron Microscopy 41
4.1.3 Fourier Transform Infrared Spectroscopy 44
4.1.4 X-ray Diffraction 46

4.2 Electrochemical Studies 48
4.2.1 Cyclic Voltammetry 48
4.2.2 Effect of Reduced Graphene Oxide 49
4.2.3 Effect of different scan rates 50
4.2.4 Electrochemical Impedance Spectroscopy 55
4.2.5 Chronoamperometry 58
4.2.6 Tafel Plot 60
4.2.7 Comparison with Literature 61

Conclusion 62

Future Recommendations 63

References 64

List of Figures

Figure 1: Typical combustion engine 2
Figure 2: Fuel cell or battery 2
Figure 3: Schematic diagram of fuel cell 2
Figure 4: Schematic of Phosphoric Acid Fuel Cell (PAFC) 3
Figure 5: Schematics of Alkali Fuel Cell (AFC) 4
Figure 6: Schematics of Molten Carbonate Fuel Cell (MCFC) 5
Figure 7: Schematics of Solid Oxide Fuel Cell (SOFC) 6
Figure 8: Schematics of Proton Exchange Membrane Fuel Cell 7
Figure 9: Schematics of Direct Methanol Fuel Cell 9
Figure 10: Schematics of various Fuel Cell Reactions 10
Figure 11: Schematic diagram of Metal Organic Frameworks 12
Figure 12: Structural design of Metal Organic Frameworks 12
Figure 13: Working scheme of XRD 18
Figure 14: Design and working principle of SEM 19
Figure 15: Working principle of FTIR 20
Figure 16: Incident and scattered energy pattern 21
Figure 17: Working principle of Raman Spectroscopy 21
Figure 18: Reaction of Graphene Oxide in ice bath 31
Figure 19: Thick paste after 48 hours of stirring 31
Figure 20: (a) Settling down of Graphene oxide with other impurities. (b) Washing and centrifugation of GO. (c) Chips of Graphene Oxide 32
Figure 21: Reflux in oil bath 33
Figure 22: (a) Boiling at 100 ^{o} C. (b) Chunks separated from suspension. (c) Dried reduced graphene oxide (rGO) 34
Figure 23: Hierarchical reaction steps for preparation of Ni-Fe MOF along with GO composites 36
Figure 24: Working electrode preparation 36
Figure 25: Dried ink on glassy carbon electrode 37
Figure 26: Electrochemical cell of Cyclic Voltammetry 38

Figure 27: Graphical representation of Cyclic Voltammetry 38
Figure 28: Graphical Representation of EIS 39
Figure 29: Scheme of chronoamperometry apparatus 40
Figure 30: Chronoamperometric graph 40
Figure 31: SEM images of (a) Ni/Fe MOF (b) 1 wt% (c) 2 wt% (d) 3 wt% (e) 4 wt% (f) 5 wt% (g) 8 wt% rGO Ni/Fe MOF and (i) GO (ii) rGO 43
Figure 32: FTIR of (a) GO (b) rGO (c) Ni/Fe MOF with rGO composites 46
Figure 33: XRD pattern of (a) GO, (b) rGO and (c) Ni/Fe MOF with its rGO composites 47
Figure 34: CV scan of bare GCE 48
Figure 35: Cyclic voltammograms of Ni/Fe MOF with rGO composites. 49
Figure 36: Cyclic Voltammogram of (a) Ni/Fe MOF with composites (b) 1 , (c) 2 , (d) 3 , (e) 4 , (f) 5, (g) 8 wt % rGO at scan rates of 500, 100, 150, 200 mV/sec in 1 M NaOH and 3 M CH_3OH. 54
Figure 37: Nyquist plot of bare GCE in 1M NaOH and 3M CH_3OH solution. 55
Figure 38: Nyquist plot of Ni/Fe MOF at different concentration in 3 M CH_3OH and 1 M NaOH solution 56
Figure 39: Comparative plot of bare GCE, Ni/Fe MOF with rGO composite 56
Figure 40: Plots of square roots against peak current densities of Ni/Fe MOF with its composites 57
Figure 41: Chronoamperometric plots for Ni/Fe MOF and with its rGO composites at scan rate of 50 mV/sec 59
Figure 42: Chronoamperometric plot for stability of a catalyst for 3600 sec in 3 M CH_3OH and 1 M NaOH solution 59
Figure 43: Tafel plots of Ni / Fe MOF with its rGO composites in 1 M NaOH and 3 M CH_3OH solution. 60

List of Acronyms

MOF	Metal organic framework	MCFC	Molten Carbonate Fuel Cell
GO	Graphene oxide	SOFC	Solid Oxide Fuel Cell
rGO	Reduced graphene oxide	AFC	Alkaline Fuel Cell
XRD	X-ray diffraction	PEMFC	Polymer Electrolyte Membrane Fuel Cell
SEM	Scanning Electron Microscopy	TGA	Thermogravimetric Analysis
FTIR	Fourier Transform Infrared Spectroscopy	DMFC	Direct Methanol Fuel Cell
MOR	Methanol Oxidation Reaction	EIS	Electrochemical Impedance Spectroscopy
ORR	Oxygen Reduction Reaction	PAFC	Phosphoric Acid Fuel Cell
HER	Hydrogen Evolution reaction	DHTA	2,5-dihydroxyterephthalic acid
CV	Cyclic Voltammetry	GCE	Glassy Carbon Electrode
DTA	Differential Thermal analysis	TEA	Tri-ethyl Amine
DMF	Dimethyl Formamide	FCC	Fluid catalytic cracking
TOE	Tons of Oil Equivalent	RE	Reference electrode
GCE	Glassy carbon electrode	OER	Oxygen evolution reaction

List of Tables

Table 1: Operating conditions and life time analysis of different fuel cells [17]. 11
Table 2: Elemental composition of rGO-Ni/Fe composites by weight percentage. 44
Table 3: Elemental composition of rGO-Ni/Fe composites by atomic percentage. 44
Table 4: Diffusion coefficients of Ni/Fe MOF and (1 wt%, 2 wt%, 3 wt%, 4 wt%, 5 wt%, 8 wt%) rGO with Ni/Fe MOF..... 58
Table 5: Comparison between different literatures and present work 61

Chapter 1

Introduction

1.1 Energy Demand

As the world proceeds, energy demands rise daily which leads to more requirement of fuel of energy sector. The main source of energy now a day is the conventional source which is used in each power sector. It mainly includes coal and gasoline. It comes with high energy density but with a fatal disadvantage of environmental pollution. The more fuel we burn, the more hazardous environment gets. The amount of CO_2 in our atmosphere increases global warming and hence destroys our environment [1, 2].

Keeping in mind of environment's health and safety, scientists and engineers worked together to incorporate those energy systems which counter the conventional depleting sources, meet the rising energy demands and most important of all, should be environment friendly. The researchers started work on different renewable energy sources to fulfil the requirements [3]. Some of the sources are listed below;

- Hydropower
- Solar energy
- Wind energy
- Biomass
- Geothermal energy
- Tidal and Wave energy
- Fuel cell

1.2 Fuel cell

Fuel cells refers to an electrochemical device which transforms chemical energy of fuel into clean and green electrical energy through redox reaction. Fuel cells are one of the answers to green energy [4]. A fuel cell is typically an electrochemical cell which converts chemical energy of a

fuel into electrical energy through redox reaction. A battery also performs same task but does not have continuous flow of fuel.

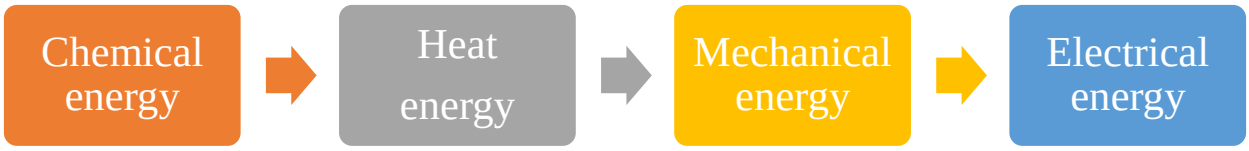

Figure 1: Typical combustion engine

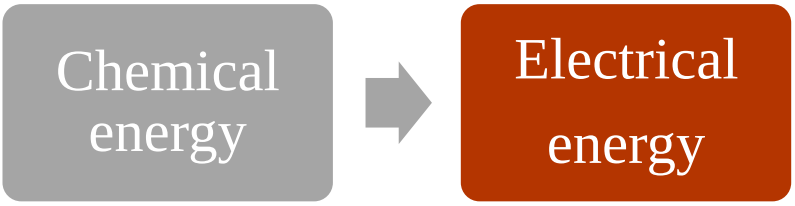

Figure 2: Fuel cell or battery

A fuel cell contains two electrodes (cathode and anode) for conducting electrons, an electrolyte (usually membrane) for ions transport and continuous supply of fuel.

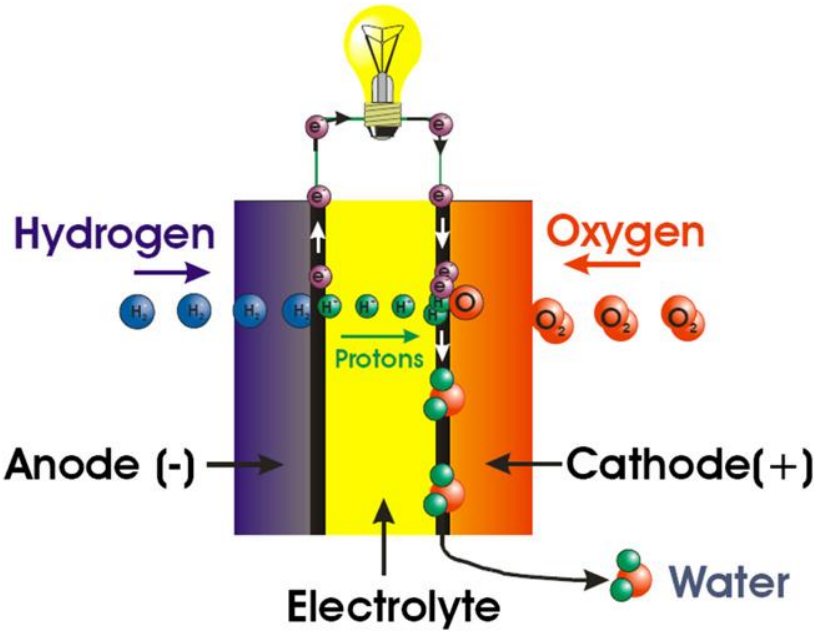

Figure 3: Schematic diagram of fuel cell

1.2.1 Types of Fuel Cell

The classification of fuel cell is characterized by their membranes, electrolytes and the chemical reactions taking place at anode and cathode of respective cell. Following are the types of fuel cell based on membrane used in them [5];

1. Proton exchange membrane fuel cell (PEMFC)
2. Alkali fuel cell (AFC)
3. Solid oxide fuel cell (SOFC)
4. Phosphoric acid fuel cell (PAFC)
5. Molten Carbonate fuel cell (MCFC)
6. Direct methanol fuel cell (DMFC)

1.2.1.1 Phosphoric Acid Fuel Cell

PAFC incorporates liquid electrolyte (either concentrated or pure) H_3PO_4 contained in a matrix of thin silicon carbide. The electrodes are made of graphite on which platinum catalyst is coated. The fuel for this type is hydrogen which enters from anode and on cathode air or oxygen is used as oxidants.

Anode

$$H_{2\,(g)} \longrightarrow 2H^+ + 2e^-$$

Cathode

$$2H^+ + 2e^- + {}^1/_2\,O_{2\,(g)} \longrightarrow H_2O_{(l)}$$

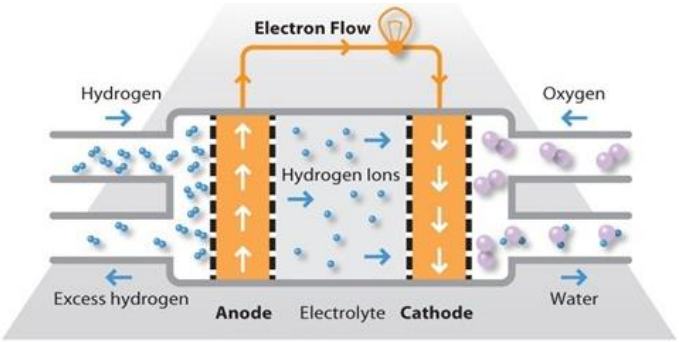

Figure 4: Schematic of Phosphoric Acid Fuel Cell (PAFC)

As the name suggests the electrolyte used is phosphoric acid but due to addition of platinum and increased temperature it is difficult to operate the cell [6].

1.2.1.2 Alkaline Fuel Cell

AFC have become mature over time. They employ an aqueous solution potassium hydroxide. Unlike PEMFC where H^+ ions are transported, in AFC OH^- ion is conducted from cathode to anode. These units were unique in a way that they were silent, produce less heat and can easily be mobilized. Due to these capabilities, AFC units were also used in NASA Apollo missions [7].

For anode

$$2H_{2\,(g)} + 4OH \longrightarrow 4H_2O_{\,(l)} + 4e^-$$

For cathode

$$O_{2\,(g)} + 2H_2O_{\,(l)} + 4e^- \longrightarrow 4OH$$

Cell reaction

$$2H_{2\,(g)} + O_{2\,(g)} \longrightarrow 2H_2O_{\,(l)} + \text{heat} + \text{electricity}$$

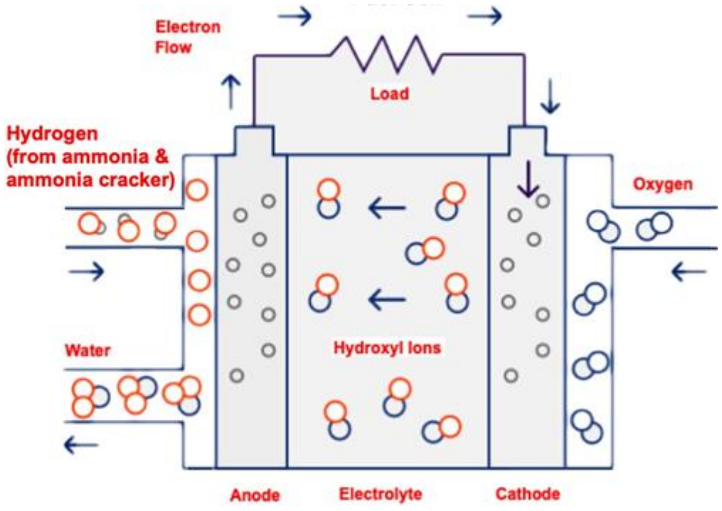

Figure 5: Schematics of Alkali Fuel Cell (AFC)

1.2.1.3 Molten Carbonate Fuel Cell

The discovery of coal brings various opportunities of production of energy. From 19th century, researches were carried out to convert coal into electricity directly using electrochemical cell. Molten carbonate fuel cell (MCFC) gave this opportunity to convert coal or its particulates

derived from petroleum, natural gas, biomass or other forms of carbon into electricity [8]. The electrolyte used in MCFC are the carbonates of molten alkali (K_2CO_3 and Li_2CO_3) which is contained in immobilized matrix of $LiOAlO_2$. The CO_3^{2-} ion acts as a carrier ion from cathode to anode [9]. Due to its intensive heat environment (600 – 700 ^oC), they are used at large scale operations with big units to produce electricity.

Anodic reaction

$$CO_3^{-2} + H_{2\,(g)} \longrightarrow CO_{2\,(g)} + H_2O_{(l)} + 2e^-$$

Cathode reaction

$$^1/_2\, O_{2\,(g)} + CO_{2\,(g)} + 2e^- \longrightarrow CO_3^{-2}$$

Cell reaction

$$H_{2\,(g)} + {}^1/_2\, O_{2\,(g)} \longrightarrow H_2O_{(l)}$$

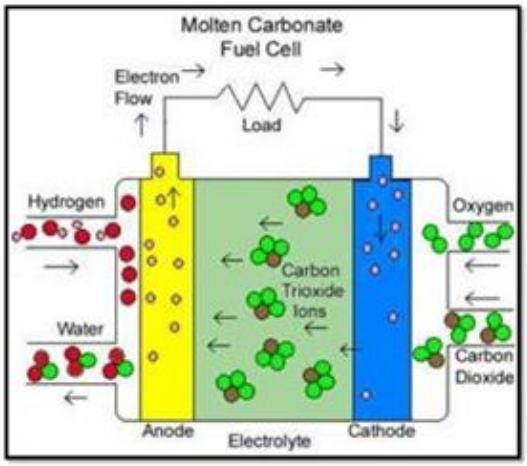

Figure 6: Schematics of Molten Carbonate Fuel Cell (MCFC)

1.2.1.4 Solid Oxide Fuel Cell

SOFCs have emerged as large operating units with the highest of operating temperature amongst all fuel cell categories. Such a fuel cell is use as a stationary or auxiliary power unit for supplying electricity. With advancement, the downsizing of SOFCs led to its application in motor vehicles specially trucks. SOFC incorporates electrolytes of solid ceramic oxides. Yttria-stabilized zirconia (YSZ) is one of the renowned electrolytes used in SOFC, which has a tendency to conduct

oxygen ions. SOFC operates at high temperatures, usually between 600 – 1000 ^{o}C. SOFCs have the highest efficiency of all the fuel cell family reaching up to 70% with an extra 20% heat recovery [10].

Anodic reaction

$$2H_{2\,(g)} + 2O^{-2} \longrightarrow 2H_2O_{(l)} + 4e^-$$

Cathodic reaction

$$O_2 + 4e^- \longrightarrow 2O^{-2}$$

Cell reaction

$$2H_{2\,(g)} + O_{2\,(g)} \longrightarrow 2H_2O_{(l)}$$

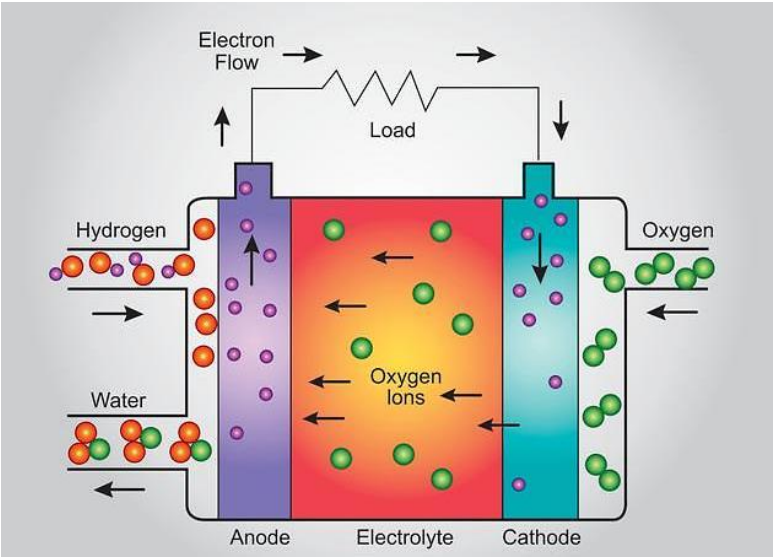

Figure 7: Schematics of Solid Oxide Fuel Cell (SOFC)

1.2.1.5 Proton Exchange Membrane Fuel Cell (PEMFC)

The readily available and commercialized form of fuel cell are proton exchange membrane fuel cell (PEMFC). PEMFC uses membrane which can conduct H^+ ions. Usually, a perfluorinated sulfonic acid is used as the polymer membrane. Platinum is used as a catalyst and coated as a thin film on membrane. Among all the fuel cell, PEMFC has the highest power density [11].

At anode

$$H_{2\,(g)} \longrightarrow 2H^{+} + 2e^{-}$$

At cathode

$$^{1}/_{2}\,O_{2\,(g)} + 2H^{+} + 2e^{-} \longrightarrow H_2O_{(l)}$$

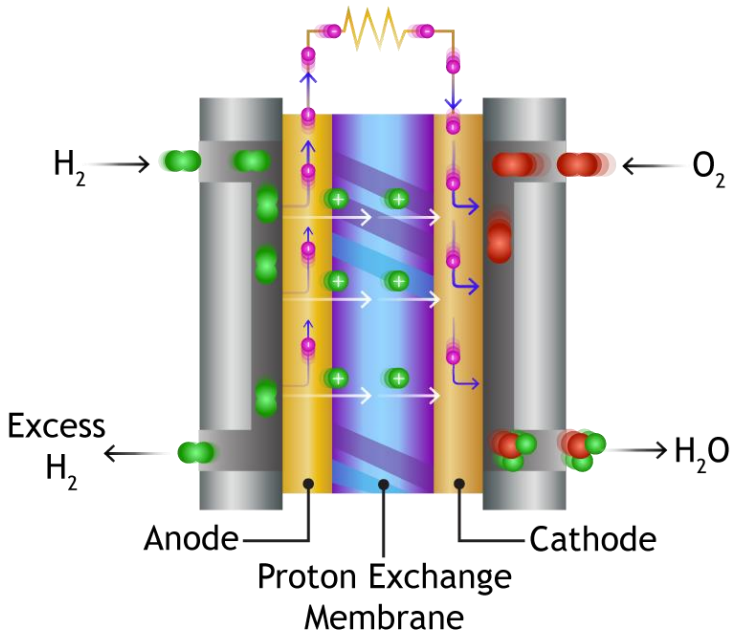

Figure 8: Schematics of Proton Exchange Membrane Fuel Cell

1.2.2 Membranes for PEMFC

The first fuel cell cation exchange organic membrane polymer was initially synthesized by GE researcher Willard T. Grubb in 1959. This membrane operated on the basic function to provide a H^{+} conducting gas barrier. For contacting medium between the catalyst surface, strong acids were used. Afterward, further development showed that fuel cell could perform well without contact layer of acid. Recent PEMFC use membrane instead of any electrolytes. In 1960s, it was found that membranes are the main component of FC because membrane in PEMFC acts as an electrolyte and PEM/catalyst interface is the controlling parameter in reaction kinetics. This gives the understanding of acid group related with FC in anhydrous form (SO_3H). When hydrated, the hydrolyzed form (SO_3^{-} H_3O^{+}) appears, which allows H^{+} ion to transport through the membrane [12].

For fuel cell applications, membrane is the vital component. The polymeric electrolyte membrane serves three major purposes;

- Transfer of H^+ ion through membrane
- separation of the reactant gases,
- Current repelling, so it passes through external circuit.

The first perfluosulphonic acid membrane was developed by DuPont in 1970s called “Nafion”, which not only enhanced the specific conductivity of H^+ ion in membrane by two-folds but also extended membrane’s lifetime by magnitude of four orders. Afterward, this became a backbone for PEMFC and till today remains the same [13].

The performance of PEM is related to its capacity of proton conduction which also extends to membrane humidity. Higher humidity leads to high conductivity. On the other hand, by reducing membrane thickness lowers membrane resistance to H^+ ions, rapid hydration and ultimately reducing cost [14].

To maintain high performance requirements for PEMFC application, proton exchange membrane should possess the following properties:

- Enhanced conductivity of H^+ ions to produce elevated current with less resistive losses.
- Negligible conduction of electrons.
- High stability and mechanical strength.
- Good stability of chemical and electrochemical reactions.
- Control of moisture in fuel cell stack.
- No by-pass of fuel or oxygen from membrane.
- Cost of production should be compatible with respective applications.

Nafion has a copolymer structure of fluoro 3,6-dioxo 4,6-octane sulfonic acid. Polytetrafluorethylene (PTFE) Teflon is the structural backbone which provides hydrophobicity to membrane and sulfonic acid groups (HSO_3^-) which is hydrophilic is grafted chemically into backbone [15].

1.2.3 Direct methanol fuel cell (DMFC)

DMFC is the sub type of PEMFC with methanol as fuel. It's one of the promising sources of energy and readily available to modern requirements. The main difficulty with these types of fuel cell is the lack of emerging technology. Previously, these fuel cells used platinum as catalyst. The answer to that is to invest in the research and look towards the new ways of designing a new catalyst that would be cheap and more effective for methanol oxidation. Although, methanol used in DMFC produce greater energy density compared to rechargeable one, cost less than alternative battery and eventually operate for longer time, but the main cost for fuel cell components is still an issue [16].

Reaction,

Anode: $CH_3OH + H_2O \longrightarrow CO_2 + 6\,H^+ + 6e^+$

Cathode: $^1/_2O_2 + 6H^+ + 6e^- \longrightarrow 3H_2O$

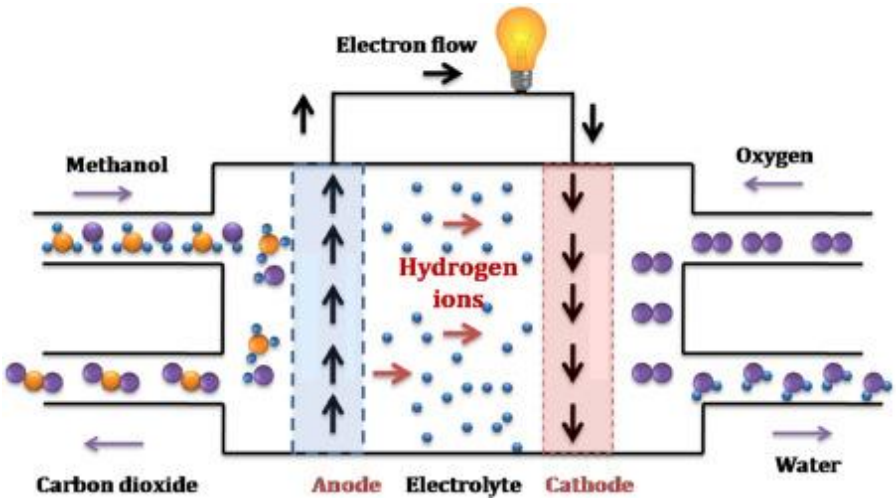

Figure 9: Schematics of Direct Methanol Fuel Cell

1.2.3.1 Challenges associated with DMFC

The membrane used in DMFC is nafion which is the same membrane used in hydrogen proton exchange fuel cells (PEMFC). It is due to its favorable and promising conditions for vehicular application and portable electronics as the use liquid fuel. Methanol is used as a source

of energy in DMFC. It consists of membrane which is packed between two electrodes. The purpose of anode is to electro-oxidize methanol into CO_2 and oxygen (present in air) reacts with H^+ ions at anode to produce water or steam.

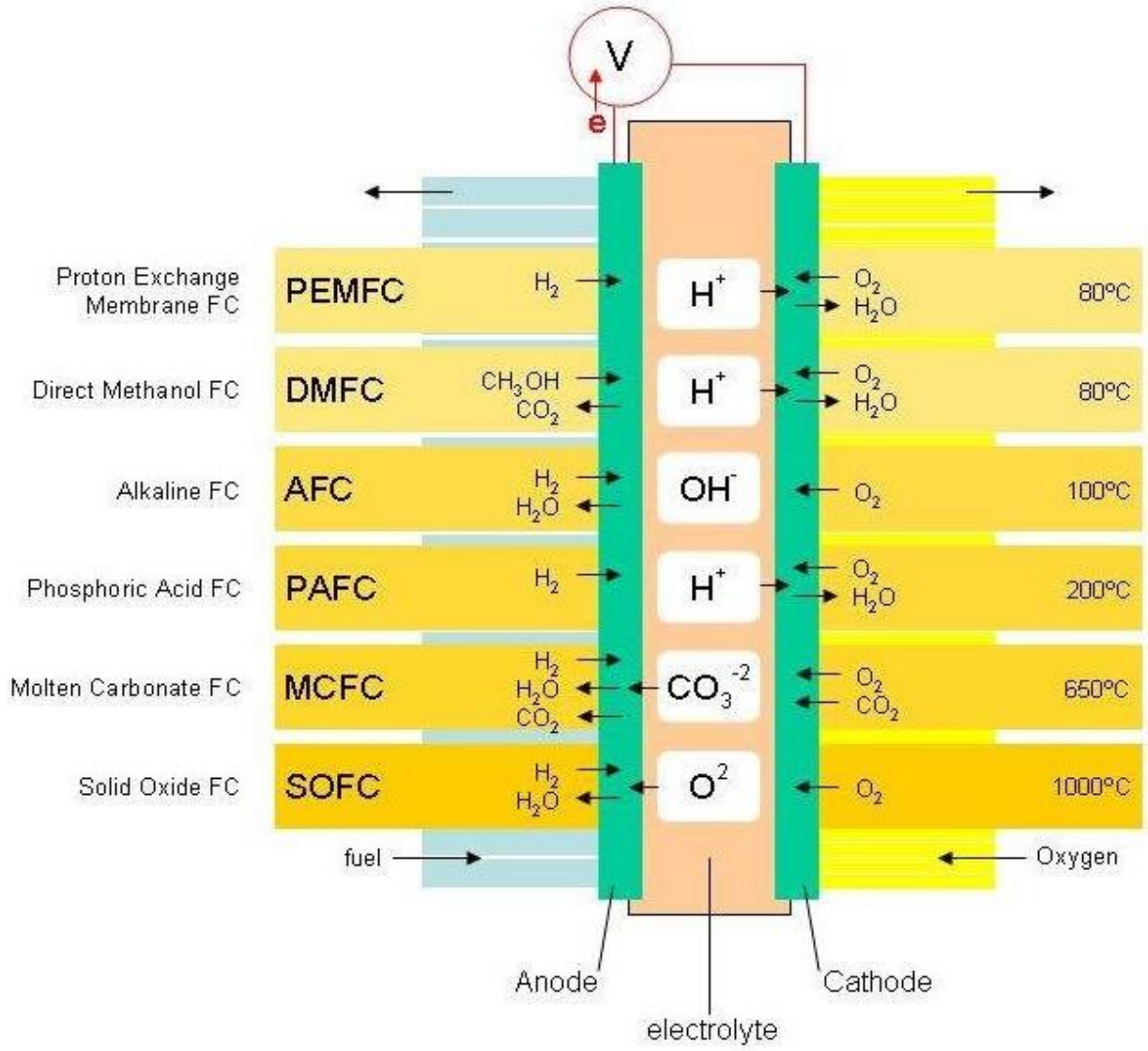

Figure 10: Schematics of various Fuel Cell Reactions

In coming time rechargeable batteries would be replaced by due to the reason that methanol possesses high energy density compared to its counterparts such as lithium-polymer and lithium-ion batteries. DMFCs can also be used as easy and quick fuel cartridge replacement. Compared to rechargeable batteries, which depend on charging for hours in case of shutdown, a DMFC can be fueled with methanol continuously [16].

Table 1: Operating conditions and life time analysis of different fuel cells [17].

Types of Fuel Cell	Operating Temperature (°C)	Power Density (mW/cm2)	Efficiency (Chemical to Electrical)	Life of fuel cell (hr)	Cost ($/kW)	Applicable areas
Alkaline fuel cell	60-90	100-200	40-60	>10,000	>200	Space, Mobile
Polymer electrolyte membrane fuel cell	50-80	350	45-60	>40,000	>200	Mobile, Stationary, Portable
Phosphoric acid fuel cell	160-220	200	55	>40,000	3000	Distributed Power
Solid oxide fuel cell	600-1000	240	55-65	>40,000	1500	Baseload Power Generation
Molten carbonate fuel cell	600-700	100	60-65	>40,000	1000	Distribution of Power Generation

1.3 Metal organic frameworks (MOF)

Metal−organic frameworks, or MOFs, are characterized as the crystalline or amorphous materials which possesses high porosity (capacity of 90% free volume) and vast internal surface area, containing beyond 6000 m^2/g. Altogether, with these properties of extraordinary variability for both inorganic and organic components and their structures, it makes MOF a potential candidate for application in green energy, most significantly in the area of gas storage for gases such as hydrogen and methane. It can also act as a good absorbent for various separation requirements. MOF are recognized by their extraordinary large surface areas, adjustable internal properties and tunable pore sizes [18]. Some other applications of MOFs include membranes for thin film, catalysis, thermal cracking and biomedical imaging. On contrary, MOF comprises the beauty and power to combine organic and inorganic compounds to form chemical structures which were regarded as two different disciplines [19].

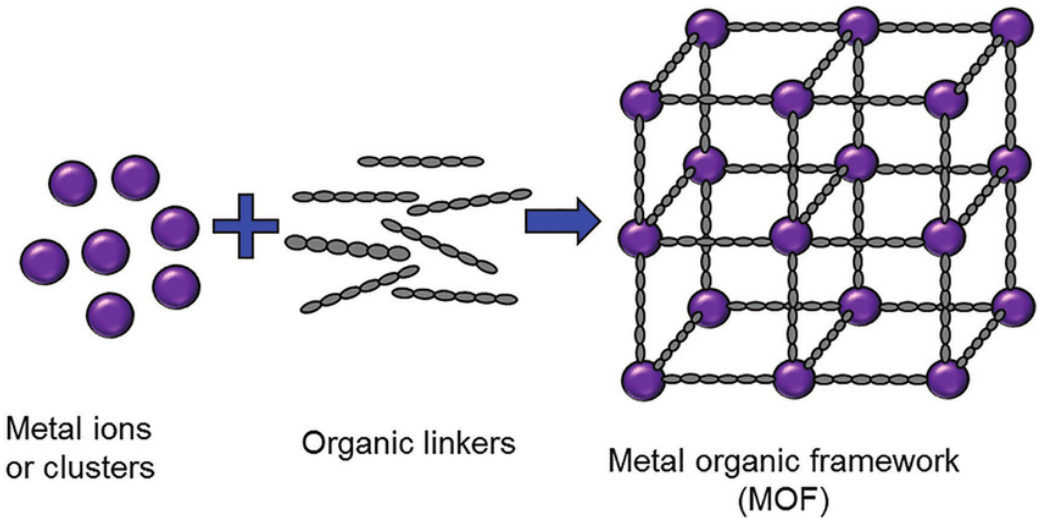

Figure 11: Schematic diagram of Metal Organic Frameworks

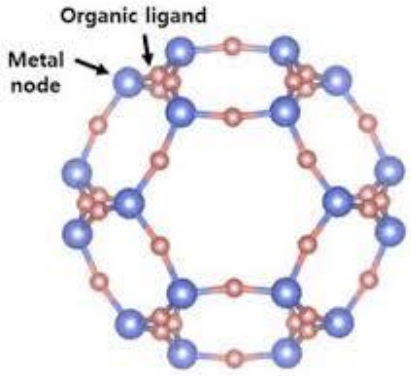

Figure 12: Structural design of Metal Organic Frameworks

1.3.1 Synthesis of MOF

Different approaches are used to synthesize MOF. Figure 11 demonstrate the components of MOF in the form of metals, slats, cluster and ligands. Most of the synthesis of MOF is carried out in liquid-based environment in which metal oxide, metal salt and ligands are mixed separately into the solution or solvent is mixed with metal salt and organic ligand simultaneously. The selection for solvent in case of these reactions depends on different properties such as solubility, reactivity, stability, redox potential etc. Thermodynamics and activation energy are also affected by employing different solvents for a particular chemical reaction. Like liquid-phased synthesis, scientist have also tested solid-phase reactions techniques for MOFs due to its relatively easy and

quick nature, but these reaction face hinderance to obtain single crystal and structure of product, that is relatively easy using liquid-phased reaction [20].

1.3.1.1 Microwave assisted technique

Microwave irradiation is the energy based, well-established technique in energetic sciences but usually applied in organic chemistry. Nonetheless, solid-based reaction as well as solution-based reaction have been described for this method. For example, synthesis of MOF and zeolites imply same techniques. The synthesis done via microwave-assisted technique relies upon the interaction between mobile electric charges and electromagnetic waves. These could be electron/ion in a solid or molecules/ion in a solution. In solids, the electric current is generated and electric resistance of solid causes heat. While in solution, electromagnetic field is formed which align polar molecules in an oscillating manner so that orientation of molecules is changed permanently. Therefore, by application of appropriate microwave frequency, vibrations between molecules take place which causes collision and leads to elevate kinetic energy such as temperature or internal energy of system. Direct interaction of microwave radiation with reactants/solution applies an energy efficient way of increasing kinetic energy. This leads to homogeneous heating and high heating rates throughout the system [21, 22].

1.3.1.2 Electrochemical assisted technique

The first MOF synthesized through electrochemical process was reported in 2005 by BASF researchers. While the MOFs can be prepared with large crystals by variation in pH of solvent under mild conditions at room temperature, the research on understanding and development of rapid and mild synthetic techniques are going on. One of the advantages of this technique is the metal salts which are no more required for production of MOFs continuously which give this technique an upper hand in industrial synthesis of MOFs. The scheme of reaction implies on provision of metal ions to anode by dissolution in synthesized mixture which includes electrolytes and linkers [23].

1.3.1.3 Mechano-chemical synthesis technique

Many physical phenomena are known to be induced by mechanical force. In some of chemical reactions they are present as well. Mechanical force is used to break intramolecular (weak) molecular forces between atoms which is followed by chemical transformation of

molecules. Mechanochemical synthesis is recently employed to multicomponent reaction (ternary or higher). These reactions produce active co-crystal for pharmaceutical applications. Mechanochemistry has been employed in parts of science like solid-state reactions, organic chemistry and polymer science. One of the important reasons for mechanically achieved MOF is that the reaction which requires solvent free conditions at room temperature. This could give advantage when working with organic solvents. The other important one is the replacement of metal salts by metal oxides. The reaction produces water as side product [24].

1.3.1.4 Sonochemical synthesis

The class of chemistry which deals with the application of ultrasonic waves in a chemical reaction is known as Sonochemistry. Ultrasonic waves are the pattern of cyclic vibrations produced mechanically between a range of frequency from 20 kHz (highest sound humans can hear) to 10 MHz. The frequency of sound waves is too high compared to molecular dimensions. Therefore, no chemical reaction proceeds directly by integration of ultrasonic waves and molecules. When a high energy ultrasonic wave interacts with solution, areas of cyclic alteration like compression (zone of high pressure) and rare fraction (zone of low pressure) are formed. For regions with low pressure, pressure drops down to vapor pressure of solution/ reactants and bubbles are formed i.e., cavities. The bubbles (micrometer size) tend to form and collapse under compression and rare fraction thus creating an interface for molecules to react [25, 26].

1.3.1.5 Slow evaporation technique

One of the conventional methods for preparation of MOFs is slow evaporation technique. It does not require external source of supply. Rather, this technique is preferred sometimes due to accessibility and ease of operating at room temperature. Although, the time required for the reaction is much more when compared with other techniques and make slow evaporation less applicable. The process of slow evaporation involves a solution of reactants, organic ligands and solvent as starting material. The materials are mixed carefully and heated slowly usually at room temperature (fixed) to concentrate the solution. More than one solvent could be applicable for better solubility of reactants which make the process faster by quick evaporation of solvents. When

the evaporation is completed, the remaining compound in washed and dried in oven to give crystalline shaped MOFs [27].

1.3.1.6 Solvothermal Method

Solvothermal technique is applied to reactions carried out in pressurized vessels above solvent's boiling point. The materials transform into nanoscale structures with the help of solvothermal technique which conventional methods cannot achieve. The solvent used in these reactions plays an important role in transforming the MOF. Some common solvents used in solvothermal technique are acetonitrile, acetone, methanol, ethanol, diethyl formamide, dimethyl formamide etc. Different temperature ranges are opted for solvothermal reaction. Mild reactions are performed in glass vials while for temperatures above 100 ^{o} C Teflon lined autoclave apparatus is required. Hydrothermal synthesis technique is the type of solvothermal technique sued successfully for synthesis of various MOFs [28, 29].

1.3.2 Applications of MOFs

- MOFs for gas storage and separation
- MOFs for electrocatalysis
- MOFs for sensing [30].

1.3.2.1 MOFs for gas separation and storage

Generally, MOF is physically characterized on its crystalline or amorphous nature. The links within structure of MOF corresponds to metal-organic linker nodes possessing large surface area, high porosity and tailored chemistry. Since its discovery in 1990s, various MOFs have been synthesized by different techniques used for gas separation and storage. For appropriate functioning of MOF, incorporation of ligands or functionalizing organic groups should be chosen carefully. For further improvement of MOFs, another metal is incorporated via new node. This is called bimetallic MOF. It has dual properties of both the metals attached to same or different ligands. In general, addition of metal node in same framework will allow more metals to incorporate with each other enhancing the defects in MOF, which is increasing

its activity, porosity and synergistic effects between metal by integration, that can boost their intrinsic properties [31].

1.3.2.2 MOFs for electrocatalysis

Catalysis is one of the main applications of metal organic frameworks. MOFs are recognized by their large porosities, diversified/tunable pore surfaces, uniform pore shape/size, redox properties and many other unique physical and chemical properties. Incorporating heterogeneous properties, MOF can possess various acidic or basic sites for catalysis with coordination structure and surrounding environment, similar to structure of that present in complexes of proteins and molecular metals. Combining the properties of molecular homogeneous and nonorganic heterogeneous catalysts, MOF can perform as a promising agent in achieving high catalytic mechanisms and performances [32].

Electrochemical reaction is one of the important parts of chemical reaction. These chemical reactions proceed by transfer of electrons directly between atoms, molecules or ions. They are often described as reduction-oxidation or redox reactions. Redox reactions are divided into two half-cell reaction of two electrodes i.e., the reduction reaction at cathode and oxidation reaction at anode. As these reactions are directly connected to clean energy conversion and storage, they are found in electrochemical devices such as fuel cells, batteries, electrolytic cells, corrosion inhibitors and supercapacitors. The reactions performed in these cells involve different half-cell reactions such as, hydrogen oxidation reaction (HOR),, oxygen reduction reaction (ORR), hydrogen evolution reaction (HER), oxygen evolution reaction (OER), sulfur reduction and sulfide oxidation, carbon dioxide reduction reactions (CO_2RR), metal ion reduction and metal oxidation, etc. [33].

MOFs incorporates large surface areas which resides in its porous structure. The structure of MOF for catalytic activity can be visualized by crystallography technique. It is important to note that solid state and solution state structures of molecules differ from each other, creating the MOFs which can be engineered according to the needs of environment. The major issue with these structures in electrochemical reactions is their low stability. Electrochemical reactions are usually performed under ionic solution or electrolyte (mainly based on water) which has high acidic or basic environment [34].

1.3.2.3 MOFs for sensing

Electrochemical sensors are considered one of the important parts of analytical instrumentation. They can be used to provide accurate sensitivity and high selectivity with relatively less expensive equipment compared to conventional techniques like atomic emission spectroscopy (AES), atomic absorption spectroscopy (AAS), chromatography (i.e. HPLC and GC) and inductively coupled plasma mass spectroscopy (ICP-MS). To achieve all those goals, one of the best options is to find biocompatible material with hybrid and multifunctional properties such as redox activities and electrocatalytic properties. Various composites of MOF such as GO-MOFs, metal oxide nps-MOFs, Ag nps-MOFs, Au nps-MOFs and CNT MOFs are enlightened with various properties to make them capable of good electrochemical and catalytic applications [35].

1.4 Characterization Techniques

1.4.1 X-ray diffraction:

XRD is one of the techniques used to determine the crystallinity of material. It gathers information about the crystallinity, orientation, layers, shape and other structural properties. A special instrument working on the principle of brags law,

$$2d \sin\theta = m\lambda$$

Where,

n = integer

λ = wavelength of X-Ray

θ = diffraction angle

D = layer spacing between crystals.

The diffraction of crystal layers is in the range of Nanometers. X-Rays are used to penetrate the crystal layers. Such an instrument operates by passing the monochromatic beam of X-Rays. The

X-Ray disperse or diffract as it strikes the crystal structure on different angles. As the result of that, sharp peaks are appeared on the graph at the angle where high crystallinity is achieved [36].

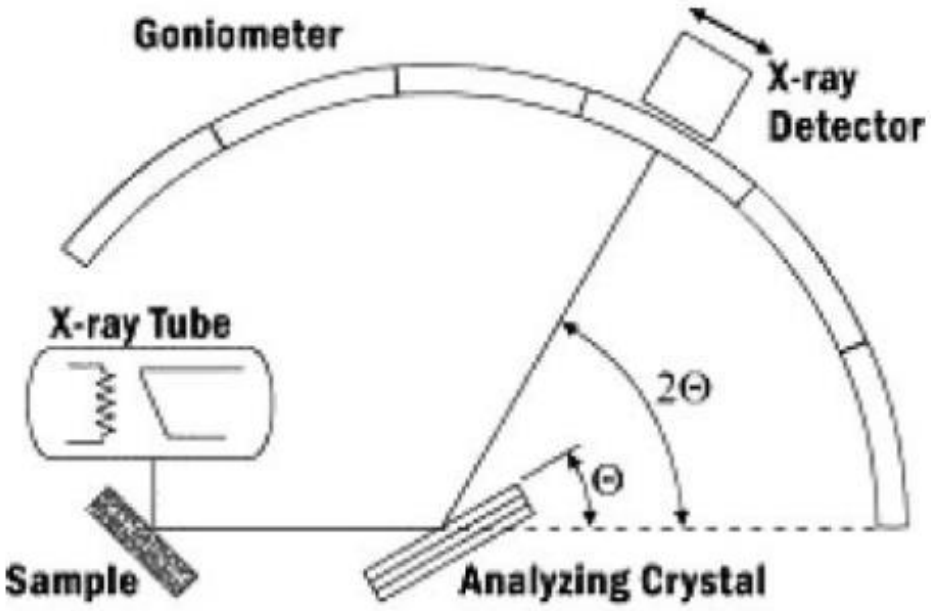

Figure 13: Working scheme of XRD

1.4.2 Scanning electron microscope (SEM)

SEM is physical analysis technique on scale up to micrometers with very high magnification. This technique is widely spread over a vast range of physical, chemical, biological sciences, engineering and technology, nano-scale structures and forensic investigations. Over a period of few decades, SEM has emerged as an indispensable tool for science and engineering. It operates on an extremely simple principle. The apparatus consists of two cathode ray tube (CRT). One of the tubes is used to place the sample which is subjected to high energy electron beam bombardment. The result of this bombardment is received by a detector and converted to signal voltage. The voltage signal is sent to grid of second CRT or display CRT [37]. Synchronous operation of both CRT produces an image which is built up, point to point on CRT display. Secondary, transmitted electrons, backscattered electrons and X-ray detectors produce the signals simultaneously which is employed as SEM image [38]. The schematic diagram of SEM is shown below;

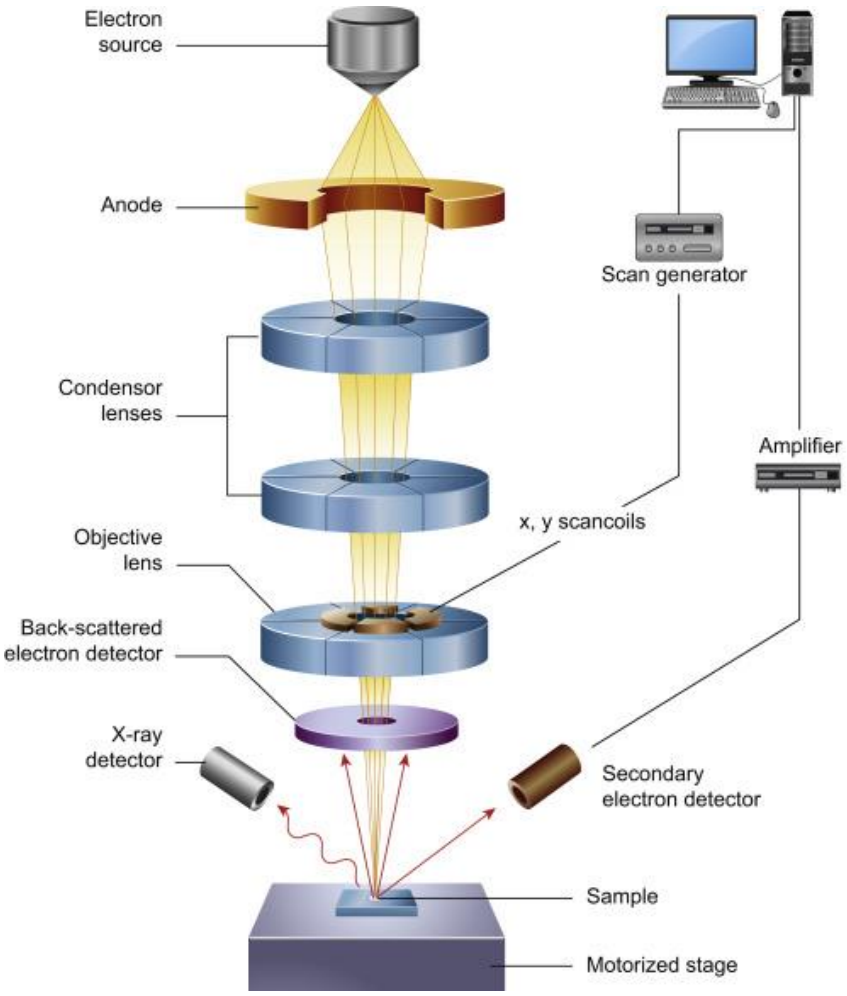

Figure 14: Design and working principle of SEM

1.4.3 Fourier Transform Infrared Spectroscopy (FTIR)

Infrared (IR) spectroscopy is a technique based on vibrations of atoms in a molecule. FTIR spectroscopy was mainly used in the middle infrared (MIR) region (4000–300 cm^{-1}) where the fundamental vibrational modes appear. The technique known as pressed discs is most utilized for routine studies. The sample is prepared by making it dispersed in KBr usually with the ratio of sample is about 1% and pressed under a disk to form pellet. Discs could be heated for about 120 ^{O}C overnight for removal of absorbed water, whose IR bands can overlap with those of the sample. The detector in FTIR spectrometers continuously monitors the full wavenumber range of radiation emitted by the IR source. Computers is required to transform this information into an

absorption/transmittance spectrum. FTIR spectrometry could be either single beam or double producing a transmittance spectrum [39].

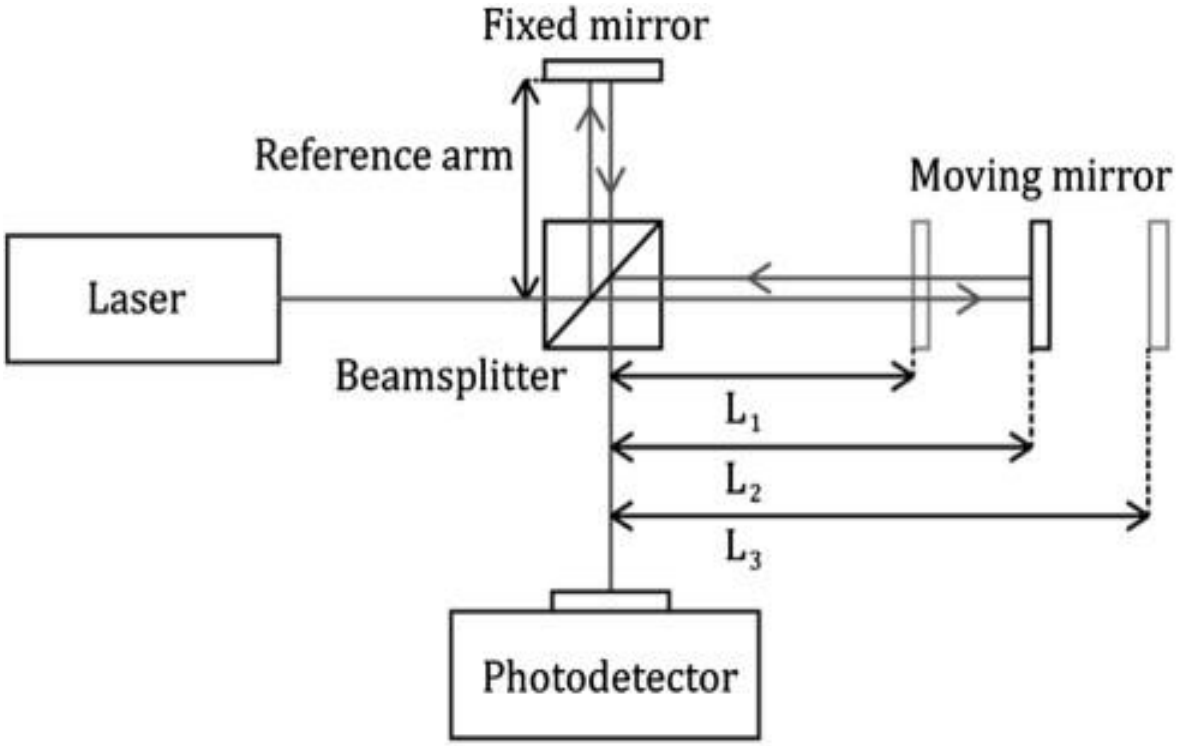

Figure 15: Working principle of FTIR

1.4.4 Raman Spectroscopy

Raman scattering was discovered by Krishna and Raman in 1928. It is a technique, which uses light scattering to collect the useful information about,

- Crystallinity
- Phase
- Morphology
- Molecular interaction
- Chemical structure

The graph of raman spectroscopy is plotted between the scattered intensity vs energy. The peaks in the graph describes the raman shift for the incident light energy [40].

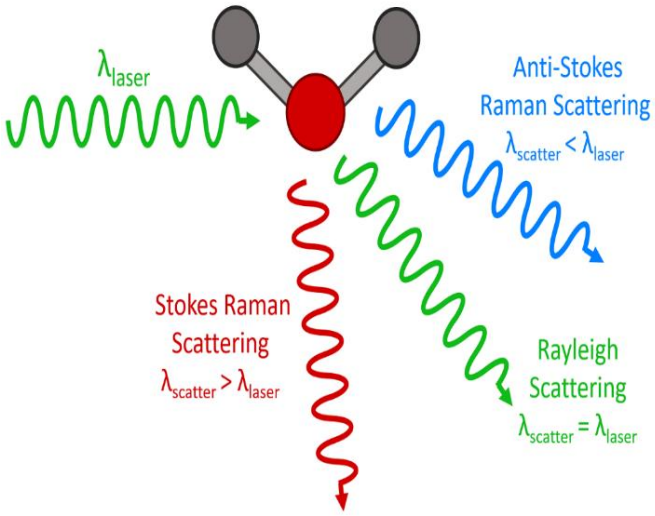

Figure 16: Incident and scattered energy pattern

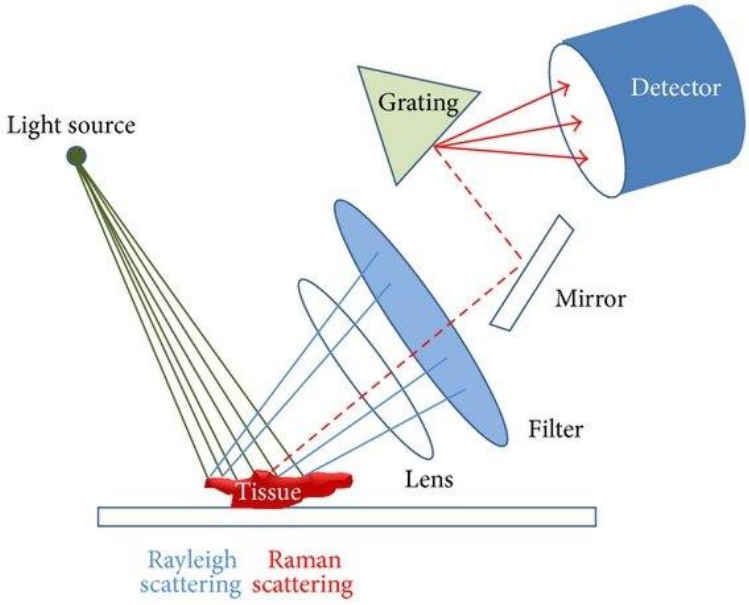

Figure 17: Working principle of Raman Spectroscopy

Like FTIR, Raman spectroscopy does also depend upon molecular vibrations. But in case of Raman the energy is scattered. On the other hand, FTIR spectrum depends upon molecular vibrations based on absorption or transmittance. Raman spectroscopy is favorable for homonuclear molecule bonds such as C-C, C=C, C≡C. The advantage of Raman spectroscopy is that it requires little to no sample preparation as compared to FTIR [41].

1.5 Catalyst for Methanol Oxidation Reaction

DMFCs have gained popularity as an effective power device due to its various advantages like low cost, high efficiency, low operating temperatures and environmental friendliness. The main hinderance for further commercialization of DMFC is the slow kinetics of methanol oxidation and oxidation reduction reactions (MOR and ORR). Since it's a subtype of PEMFC, it uses the same catalyst that is Platinum. But Pt is a noble metal and can be prone to catalytic poisoning. Therefore, a catalyst which is non-noble, incorporates anti-poisoning abilities and can easily oxidize methanol is desired highly. For that case, introduction of non-precious transition metals (such as Co, Fe, Cu, Ni) have arrived in researchers mind to boost performance of catalyst. Previously, transition metals were used as promotors (oxides and phosphides) with Pt catalyst to promote methanol oxidation. For further increment in performance of catalyst, surface engineering like metal-support interaction, surface doping and core-shell structure have been synthesized for modification of platinum. Currently, Pt-Ru is regarded as best performing catalyst [42].

- Pt-Ag possess good activity for electrochemical reactions. The bimetallic catalyst shows high activity towards formic acid, ethanol and methanol oxidation compared to Pt/Ru-C or Pt/C which are commercially available [43].

- There is a chance of strong interaction present between platinum catalyst and TiO_2 nanotubes. As the Pt particles are dispersed on TiO_2, it gives high electroactivity of platinum compared to other substrates on which Pt is dispersed. The merger of these two catalysts enhance activity of catalyst for MOR. [44].

- Graphene oxide, reduced graphene oxide, single walled carbon nanotubes (SWCNTs) and multiwalled carbon nanotubes (MWCNTs) are used as support for the catalyst in acidic environment.

The other way to improve electrochemical activity for DMFC is the use of transition metal or non-precious alloys. Many transition metals have been synthesized before used for MOR reaction such as Ni, Cu, Mn, Co, Fe etc. most popular of them are Ni and Fe nanostructures. These elements have gained researchers' attentions due to certain low cost and catalytic activity under given circumstances such as decomposition, partial oxidation, reformation, hydrogenation and electrocatalysis [45].

1.6 Research Objectives

The objectives for the given project are based on following points:

- Synthesis of graphene oxide (GO) by Hummers' method.
- Reduced graphene oxide (rGO) synthesis by chemical reduction technique.
- Synthesis of bimetallic Ni-Fe MOF with the help of hydrothermal method.
- Synthesis of rGO and Ni-Fe MOF composites.
- Characterization of synthesized samples using FTIR, XRD, SEM and EDX analysis.
- Electrochemical studies using electrochemical impedance spectroscopy (EIS), cyclic voltammetry (CV) and Chronoamperometry.

Chapter 2

Literature Review

T. Noor et al. Novel catalyst of bi-metallic (MOF), Nickle oxide and Copper oxide was developed by using organic linkers pyrazine ($C_4H_4N_2$), benzene dicarboxylic acid (BDC). To support electrochemical reactions along with bi-metallic MOF, its composites were made along with reduced graphene oxide (rGO). SEM, EDX, XRD, FTIR, Raman spectroscopy, TGA and BET analysis were conducted for physical properties. The Ni-Fe composites were tested for electrochemical studies of cyclic voltammetry (CV), for 3M solution of methanol. The composite gives a promising current density of 437.28 mA/cm^2 at 50 mV/sec and 0.9 V [46].

L. Yaqoob et al. Ni-BTC MOF was prepared along with the composites of 1, 2, 3, 4, 5 and 8% rGO by solvothermal technique. SEM, EDX, XRD and FTIR analysis were conducted for physical properties. Modified glassy carbon electrode was used as working electrode. Methanol oxidation reactions were conducted at 2M MeOH solution with 1M NaOH as support electrolyte. The best results were concluded by Ni-BTC/4 wt% rGO of about 200.22 mA/cm^2 given 0.69 V and 50 mV/sec. with the increase in amount of catalyst, the current density is gradually increased until 2 mg, which was recognized as ideal concentration for further procedures [47].

X. Shi et al. Zeolitic Imidazole Framework (ZIF) is a branch of MOF and is a potential candidate due to its high surface area with conducting networks. For this paper, noble Pt-Co catalyst with Nitrogen doped Carbon Nanotubes (Pt-Co/NCNT) was synthesized through pyrolysis of ZIF-67 with Pt precursor in Ar-H_2 environment. Study of rotating disk electrode for oxygen reduction reaction was evaluated at 70 ^{o} C with Nafion-212. The observed peak of 630 and 560 mW/cm^2 respectively for Pt-Co with CNTs and Commercial Pt/C [48].

R. Mehak et al. reported Co-MOF-71 and its composites with rGO through hydrothermal method. They also characterize their prepared samples by FTIR, XRD, SEM and XPS. They analysed chemical activity of catalysts for MOR by using three electrode systems: working electrode

(modified GCE), reference electrode (Ag/AgCl) and counter electrode (Pt wire) in basic medium (1M NaOH + 3M CH_3OH). A significant peak current density (29.1mA/cm^{-2}) was observed at potential 0.1V. These results make it a capable substance for fuel cell application for MOR [49].

Yueming Li.et al worked in a simple technique for Pt nanoparticle distribution on graphene composites. Electrochemical studies were carried out in 0.5 M CH_3OH and acidic medium of 0.5 M sulfuric acid. The results showed better catalytic activity of Pt graphene composites compared with Pt-vulcan catalyst. The catalyst gives better stability and a current density of 199.6 mA/mg at potential of 0.652 V which was twice the results compared to Pt-vulcan catalyst with 101.2 mA/mg at 0.664 V proving it a promising catalyst for methanol oxidation in DMFCs [50].

Xingcheng Ma et al. reported in situ synthesis of copper-nickel metal nanoparticles consists of a bimetallic MOF by engraving two non-noble metal component nanoparticles for OER. The encapsulation of metal nanoparticles provides appreciable conductance and stability to MOF along with providing active sites of metal for enhanced activity of oxygen evolution reaction. This bimetallic system provides better efficiency as compared to the monometallic systems due to synergic effect. The current density was improved to 1.48, 1.60 and 7.18 times in contrast to the Ni-MOF-74, Cu-Ni seeds and Cu-MOF-74 at an over potential of 624 mV respectively [51].

Y. Huang et al. reported formation of Pt nanoparticles by two-step fast microwave assisted polyol process. They reduce Pb^{+2} ions into Pb atoms for alloy formation with Pt at high temperature with the aid of microwave energy. They characterized prepared catalyst through XRD and TEM which showed core shell of Pt in Pt-Pb catalyst produced at the end of the reaction where exhaustion of Pb^{+2} ions resulted. Core was a Pt nanoparticle where shell was made up of completely alloyed nanoparticles of Pt-Pb. Catalysts' average diameter was recorded as 5.9 nm [52].

Z.K. Ghouri et al reported 4nm sized nano-engineered ZnO/CeO_2 dot at CNFs which had high dispersibility on the surface of CNFs and this dispersion enhanced its methanol activity making it a competitive and non-precious candidate for DMFC application. They synthesized these nanodots

with two ratios of $ZnO_{(60\%)}$ / $CeO_{2(40\%)}$ dots and CNFs and $ZnO_{(40\%)}$ / $CeO_{2(60\%)}$ dots at CNFs which gave value of peak current density as 5.3 mA/cm^2 and 16.3 mA/cm^2 respectively at scan rate of 50mV/s [53].

M. S. Rahmanifar et al. co-synthesized Ni-MOF and Co-MOF as previously reported method within the same reaction vessel along with the synthesis of Ni/Co-MOF-rGO nanocomposites by following the same procedure with admirable performance of supercapacitance with specific capacitance value of 850 F/g at 1 A/g. High specific energy with the value of 72.8 Wh/kg was obtained with asymmetric rGO composite with Ni-Co MOF with value of current density 1 A/g with excellent specific power of 42.5 kW/kg and 50 A/g and bearing high specific capacitance value of 181.4 F/g at 1A/g and exhibit high stability at 91.6% retention of capacitance after running 6000 cycles [54].

S. S. Mahapatra et al reported electrochemical synthesis of Pt-Pd/C catalyst which depicts high efficiency against methanol oxidation in basic medium. They studied different methanol concentrations on Pt-Pd/C catalyst and observed high peak current density with the increase in concentration of methanol. Appreciable increase in peak current density was observed till 1.0 M methanol concentration. A linear increase in energy value was also observed with increase in concentration of NaOH so optimum ratio for MeOH/NaOH was 1:2 recorded. They reported reaction order of 0.45 and 0.70 for methanol and NaOH respectively. R_{ct} (2.38 Ω) and low value of Tafel slop showed that Pt-Pd/C is a promising catalyst for application in DMFC in basic medium [55],

M. K. Jeon et al. reported Pt/WC catalyst and analysed its physical and electrochemical characteristics. Pt/WC showed low peak potential of 0.68 V when compared with Pt/C catalyst which had peak potential value of 0.80 V. They also calculated surface area from H^+ and CO desorption which gave the values of 11.2 and 5.74 m^2/g catalysts, respectively, which clearly indicate spill over of H^+ occurs in Pt/WC. It showed 30% better efficiency with 188 mA/m^2 peak current density in contrast to commercially available Pt/C catalyst which showed current density value of 144 mA/m^2 [56].

T. Noor et al. reported Cu-MOF synthesis and its GO composites with different weight percentages of graphene oxide (GO). The prepared 3D metal organic framework showed appreciable electrocatalytic activity for MOR. Among all prepared catalysts, 5wt% GO/Cu-MOF showed highest activity with peak current density of 10 mA/cm^2 at 0.8V potential. The current density of this catalyst was analogous to commercially available Pt/C catalyst but stability needs to be improved by further modification. Due to comparable results with Pt based catalyst, it could be served as economical alternative to the expensive catalysts in DMFC with commercial feasibility [57].

J. Lan et al. reported trimetallic Pt-Ni-Cu nanoalloys for methanol oxidation showing that introduction of diminutive amount of Ni over Pt-Cu alloys could improve the efficiency and stability of MOR. Their work showed that Ni-doped Pt-Cu nanoalloys were effective electrocatalysts for DMFC in acidic medium. $Pt_{60}Ni_3Cu_{37}$ showed best catalytic performance and 12% mass loss observed through chronoamperometry while $Pt_{60}Ni_{13}Cu_{27}$ showed 27% loss in mass and less efficient as compared to the previous one. Moreover, commercial Pt black and porous $Pt_{55}Cu_{45}$ were also compared with $Pt_{60}Ni_3Cu_{37}$ which showed less efficiency [58].

H. Ramezanalizadeh et al. reported synthesis of novel $BiFeO_3$ on the Co/Ni MOF composite which was magnetic, durable, highly effective photocatalyst by adopting facile approach and confirmed their synthesis by using SEM, XRD, FTIR, DRS, VSM, BET, EDX and TEM. They also observed different experimental parameters. Results showed that $BiFeO_3$ (1:1) proved highly efficient photocatalyst for MOR and 4-NP contaminants degradation by using placid conditions. When magnetic was $BiFeO_3$ immobilized on Co/Ni-MOF, it showed enhanced activity of the catalyst in all aspects [59].

I. Danaee et al. reported the deposition of NiO film electrochemically on Ni and Ni/Cu alloy on GCE and tested for impedance studies of electrochemical MOR in basic media. Two semicircles were reported with positive resistance for GC/Ni subsequent to R_{ct} and adsorption of intermediates while negative resistance was reported for impedance plots of GC/Ni-Cu. Impedance data was analysed at various potentials which gave evidence for occurrence of both simultaneous

processes at interface i.e., intermediate formation as a result of methanol oxidation and the other is oxidation of those intermediates. Varied potential also showed variations in mechanism and rate-determining step. Meanwhile, rate determining step of MOR intermediate potential was observed in transition range [60].

V. Radmilovic et al. reported three conclusive results from the analysis of carbon supported Pt-Ru electrocatalysts by utilizing the contrast of XRD and HR (high resolution) analytical electron microscopy. Firstly, particle size was affected a little by the existence of Ru in the catalyst giving an average size of particle of about 2-3 nm for 3:1 and 1:1 Pt-Ru catalysts similar to the particle size of Pt particles supported on same substrate. Particle size distribution Pt-Ru by HREM for 90% particles was ±0.5 nm for 3:1 and ±0.2 nm for 1:1. Secondly, uniform composition was observed for the particles but they were failed to determine the presence of surface segregation in the individual crystals if any. Thirdly, mostly particles were observed in cubic-octahedral shape by the presence of (111) and (200) crystallographic planes as also observed in pure Pt and many fcc metal nanocrystals. Sporadically (113) types facets were also observed that were not fcc type nanocrystals and did not appear in case of pure Pt particles on same support [61].

The thorough study of research work done until now for the betterment of DMFC activity and stability opened many new routes as well. From the literature, we can see that there are still some fields through which we can expand the studies and research. Some of the areas unexplored until now are;

- No work has been done with catalyst without containing Pt as a component for DMFC.
- Metal organic framework has never been tested for MOR in DMFC
- Composites with GO have been tested for evolution reactions and reduction reactions but they are not been used for methanol oxidation purposes
- Very less effort has been done to improve the values of potential or voltage towards lower values.

Chapter 3

Experimental Section

This section elaborates the experimental work carried out in different laboratories and incorporates various suitable synthesis methods used to synthesize desired product. This section describes the synthesis techniques required to produce the desired product as well as the design of cell assembly used to conduct electrochemical studies.

3.1 Synthesis of bimetallic Ni-Fe MOF

3.1.1 Materials

$Ni(NO_3)_2.6H_2O$ (Nickel nitrate hexahydrate), $C_4H_4N_2$ (pyrazine), (ferrous nitrate hexahydrate) $Fe(NO_3)_2.6H_2O$, 2,5-dihydroxyterephthalic acid (DHTA) , N, N-dimethylformamide (DMF) and ethanol (C_2H_5OH). All materials were received from sigma-Aldrich and Merck and were utilized in their original shape.

3.1.2 Equipment

Teflon lined autoclave, Hot plate, centrifuge machine and vacuum oven.

3.1.3 Method of preparation

Preparation of MOF led to difficult techniques. From some of them, hydrothermal technique was used as a favorable technique to derive bimetallic MOF in which problems are omitted such as non-aqueous precursor solution and high boiling point solvent [46].

- 2 mmol of pyrazine and 1mmol of terephthalic acid were dissolved in 14ml of dimethyl formaldehyde and continuously stirred.
- Metallic salts of equimolar (1mmol) $Ni(NO_3)_2.6H_2O$ and $Fe(NO_3)_2.6H_2O$ was mixed into the previous solution and allowed to continuously stir till all the crystal materials were dissolved and form homogeneous solution.

- The homogenous solution was poured into Teflon coated autoclave in which it was heated at 200 ^{o} C for 48 hours.
- Blackish powdered material was obtained as a product.
- The product was then shifted into the beaker and the settled crystal were separated.
- The sample was then washed five times with ethanol to remove any unreacted material.
- Vacuum oven was used to dry the sample at 45 ^{o} C [62].

3.2 Synthesis of Graphene oxide

Hummers and offeman proposed a technique in 1958, which has been employed for lab synthesis of Graphene oxide [63]. This technique used graphite powder as raw material and chemically reacted it with oxidizing agents to form exfoliated graphene oxide (GO).

3.2.1 Materials

- Concentrated Sulfuric Acid (98% H_2SO_4),
- Graphite Powder,
- Potassium Permanganate ($KMnO_4$)
- Hydrochloric Acid (37% HCl)

  These chemicals were purchased from Sigma Aldrich.

$NaNO_3$ (sodium nitrate) was acquired from BDH whereas H_2O_2 (hydrogen peroxide) was provided by Merck. DI from Sigma Aldrich water was used throughout the experiment for filtration.

3.2.2 Equipment

Pyrex beaker, Hot plate, magnetic stirrer, vacuum oven, centrifuge machine, vacuum filter.

3.2.3 Method of preparation

A Pyrex beaker of 500 ml was taken and poured with graphite powder and $NaNO_3$ in ratio 2:1. The concentrated H_2SO_4 (98%) was used as an oxidizing agent along with $KMnO_4$ and $NaNO_3$.

- Graphite powder (2g) along with $NaNO_3$ (1g) and H_2SO_4 (50 ml) where rotated via magnetic stirrer on a hot plate. The reaction was exothermic therefore experiment was conducted under an ice bath. The temperature of the sample was suppressed up to 0 ^{o} C. The reaction was vigorously stirred for about 2 hours to start oxidation. Afterwards, 6 g of ($KMnO_4$) was added into the reaction. $KMnO_4$ addition could trigger temperature rise, therefore it was added pinch by pinch to avoid it. The temperature was held between 0 – 5 ^{o} C.

Figure 18: Reaction of Graphene Oxide in ice bath

Figure 19: Thick paste after 48 hours of stirring

- The temperature of the sample was kept under 35 – 40 ^{o} C. The ice bath was removed so the sample is mixed at moderate temperature. The stirring of solution was kept up to 48 hours, so the maximum oxidation of graphite is achieved. The resultant solution became highly viscous like a thick paste.

- After 48 hrs. of stirring deionized (100 ml) was added in the solution drop wise. The water addition starts oxidation of graphite and reaction becomes exothermic. The temperature must be kept under 90 ^{o}C to avoid any hazard. Afterwards, 200 ml of water is added again to dilute concentrated H_2SO_4.
- Finally, H_2O_2 (10 ml) was added to stop oxidation. The solution was kept for stirring till 30 min. The final color of the sample becomes yellowish brown.
- The solution was shifted from stirring and product was settled. The settled product is washed by 0.1 M HCl (10%) to remove metal ions.
- Finally, the settled product was centrifuged with deionized water several times up till the pH of GO closes 6-7.
- GO is dried at 35 ^{o} C in vacuum oven to remove any moisture. The resultant product is dried graphene oxide [64].

(a) *(b)* *(c)*

Figure 20: (a) Settling down of Graphene oxide with other impurities. (b) Washing and centrifugation of GO. (c) Chips of Graphene Oxide

3.3 Synthesis of reduced graphene oxide (rGO)

Reduced graphene oxide was synthesized by using reported approach using modified hummers method. Hydrazine hydrate was used to chemically exfoliate the substance.

3.3.1 Materials

- Graphene oxide.
- Hydrazine hydrate (NH_2NH_2. H_2O)

3.3.2 Method of preparation

- 100 mg of graphene oxide was mixed with 100 ml of deionized water and sonicated for about an hour to get a suspended solution of brown color,
- The suspension was poured into a round bottom flask. 1 ml of hydrazine hydrate was added to the suspension.

Figure 21: Reflux in oil bath

- The suspension was boiled at 100 ^{o} C for about 24 hours under reflux in oil bath. This allows uniform heating of suspension and minimum loss of suspension.
- Black flocculent kind of chunks of rGO which are being hydrophobic started to separate from the mixture gradually.
- Product was then separated and filtered under vacuum with the help of quantitative filtration membranes.

- Finally, the product was washed using methanol and deionized water then dried under vacuum at 60 º C [65].

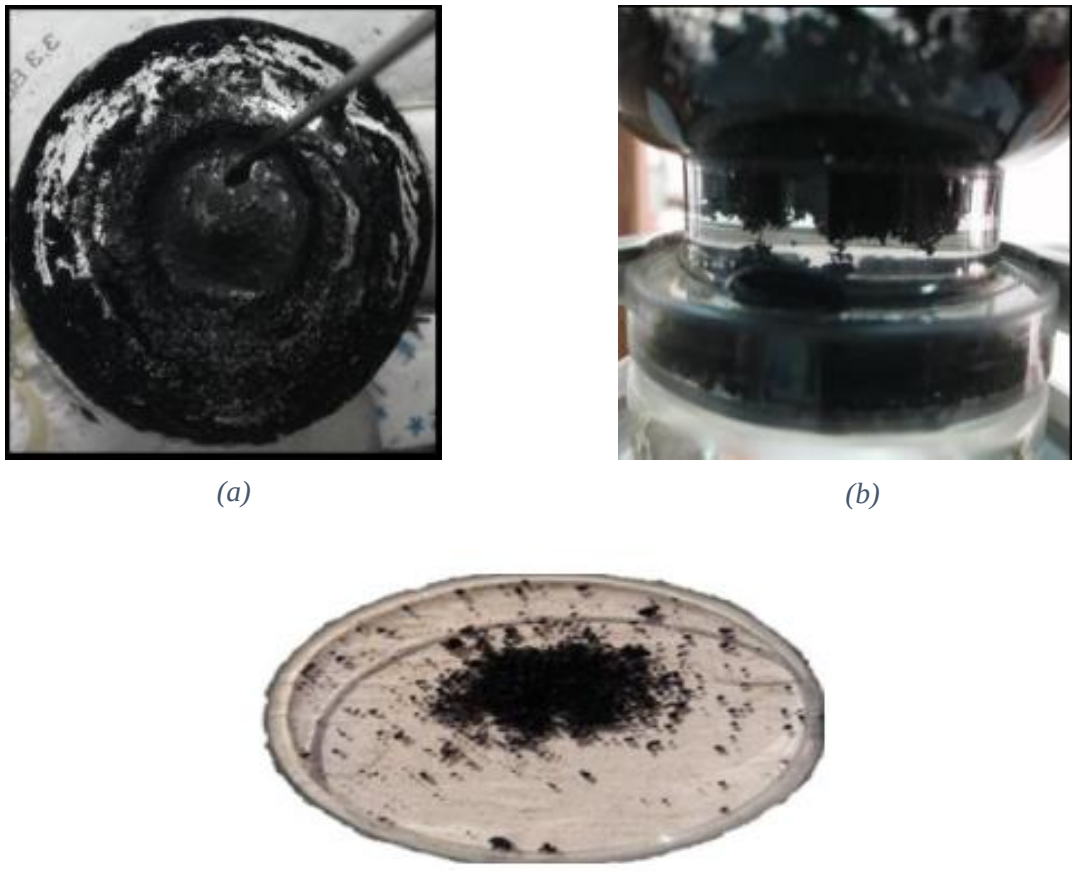

(a) *(b)*

(c)

Figure 22: (a) Boiling at 100 º C. (b) Chunks separated from suspension. (c) Dried reduced graphene oxide (rGO)

3.4 Synthesis of rGO-Ni/Cu MOF composites

Similar method (hydrothermal) was applied for the synthesis of Ni - Fe MOF and the resulting crystals were generated.

- 2 mmol pyrazine and 1 mmol DHTA were mixed in 14 ml of DMF and a solution as achieved.
- Equimolar salts of 1 mmol $Ni(NO_3)_2.6H_2O$ with $Fe((NO_3)_2.6H_2O$ each were added and continuous stirred till the solution becomes homogenous.

- On other side, reduced graphene oxide (rGO) was sonicated for 1 hour to produce fine suspension.
- The pre-sonicated suspension was added into the solution and stirred for 2 more hours.
- After completion of stirring, solution was poured into Teflon lined autoclave and heated up to 200 ^{o}C for 48 hours.
- The washing of final product was done by ethanol several times to remove any impurity and unreacted particles proceeded by centrifugation and drying at 55 ^{o} C.
- Following the same procedure, different composites were prepared by changing the wt% of rGO which is (1 – 5 and 8) wt%.

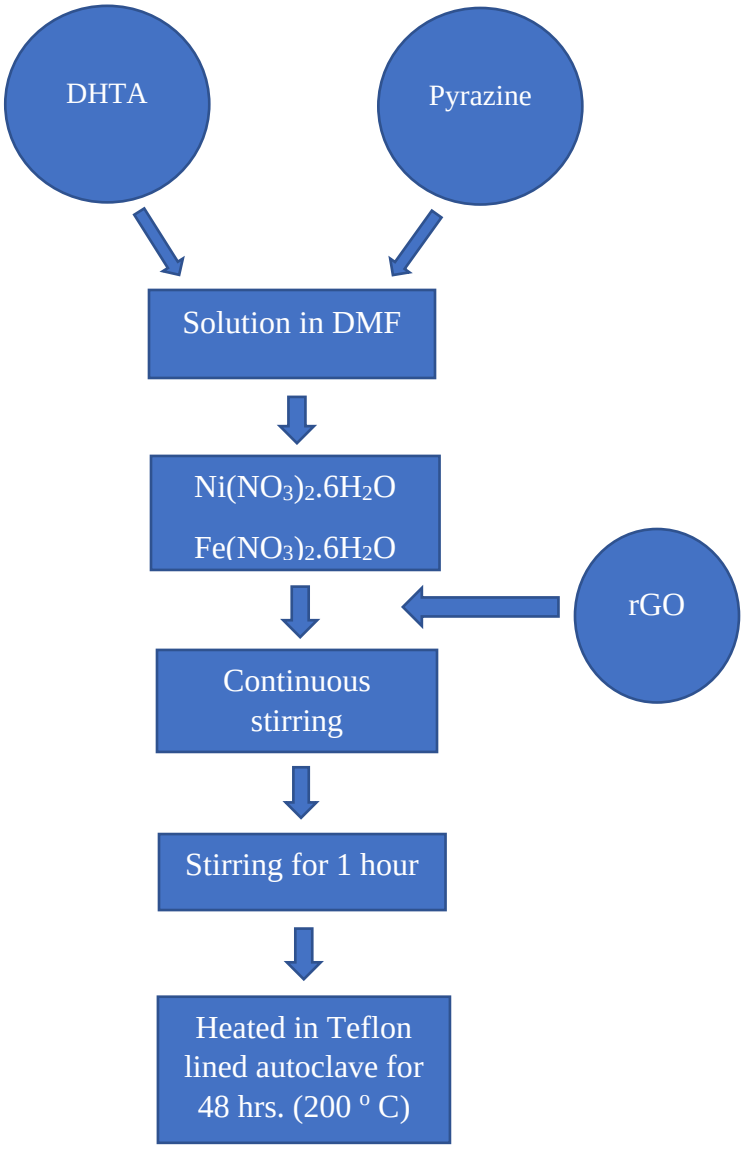

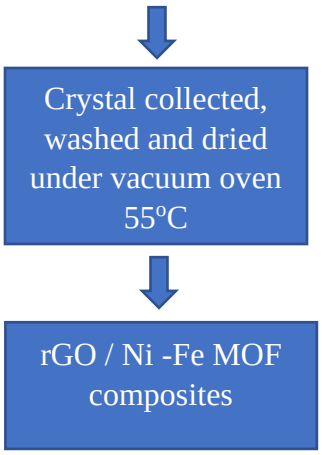

Figure 23: Hierarchical reaction steps for preparation of Ni - Fe MOF along with GO composites

3.5 Preparation of modified working electrode

For electrochemical studies to be carried out, an ink is formed. For this purpose, specific amount of catalyst i.e., 3 mg, 20 µl of nafion and 100 ml of ethanol were mixed together and sonicated for about an hour to thoroughly develop interaction between nafion and catalyst material. It forms a black ink which is loaded over glassy carbon electrode surface very carefully with the help of micropipette. It is deposited in such a way that the surface area of GCE is completely covered by the ink.

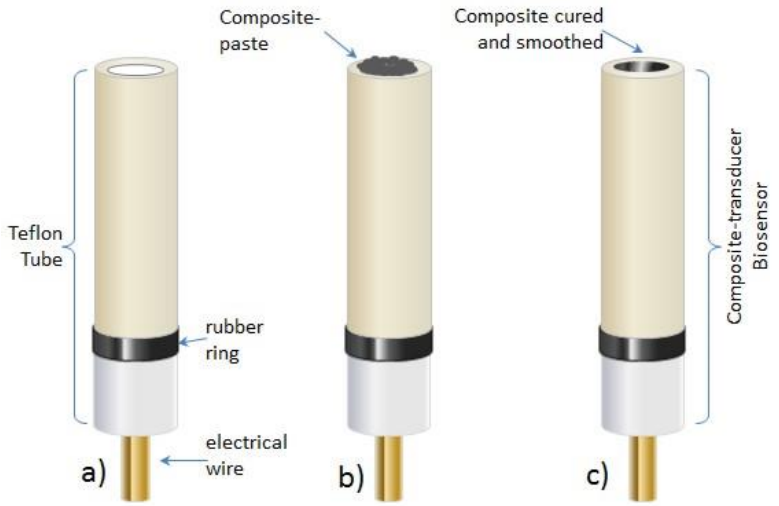

Figure 24: Working electrode preparation

The surface is then dried so that the ink absorbs on the surface and does not drop out into the solution. A thin film is adhered on the surface and the electrode is prepared for electrochemical studies. Previously, different weight percentage of rGO along with Ni-Fe MOF were prepared. These bimetallic MOFs were studied under different scan rates and concentrations so the best possible one can be selected [57].

Figure 25: Dried ink on glassy carbon electrode

3.6 Electrochemical testing techniques

3.6.1 Cyclic voltammetry

CV provides versatility and ease in inquiring about electrochemical species. It has extensive use inorganic chemistry, inorganic chemistry, biochemistry and electrochemistry. The potential of effectiveness for CV lies in its capability to scan rapidly and observe redox reaction over catalytic surfaces. The CV apparatus relies of potential cycling on an electrode, which is dipped in acidic or basic solution. The potential is caught on working electrode. Reference electrode provides control over potential coming toward working electrode. These potentials create an exciting signal which is plotted in cycles onto the graph. In this way a cyclic voltammogram is produced which presents current measure during voltage scan. CV graph is the plot of current produced against the

potential applied towards the electrode. The scan starts with negative cycle, calculating parameters of reduction and then starts positive cycle for oxidation reactions [66]. A schematic diagram of CV is shown in figure below along with its graph.

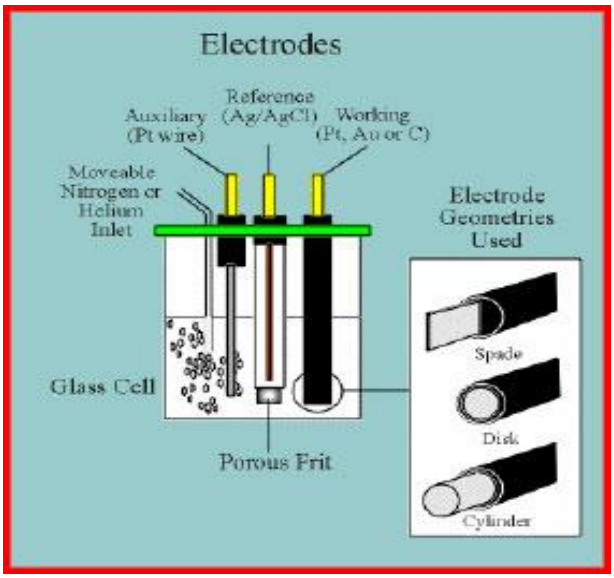

Figure 26: Electrochemical cell of Cyclic Voltammetry

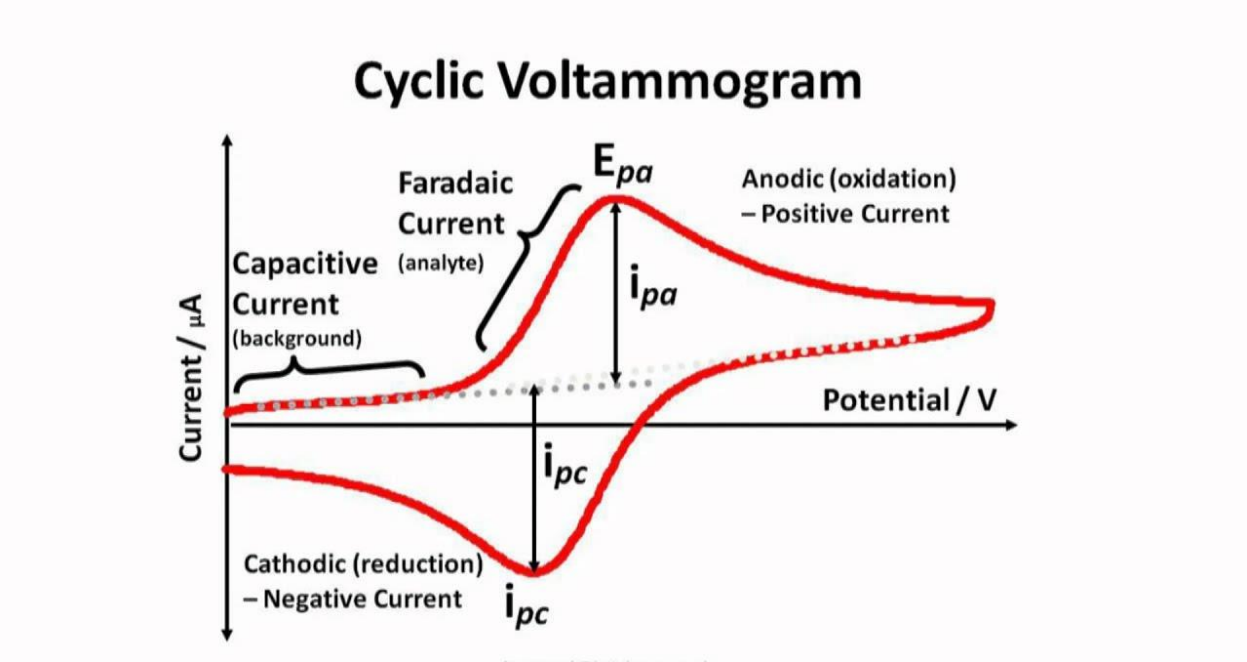

Figure 27: Graphical representation of Cyclic Voltammetry

3.6.2 Electrochemical Impedance Spectroscopy

AC impedance or EIS in recent years have gained tremendous popularity. Previously used for determination of double layer capacitance and AC polarography, it is now used as characterization technique for electrode processes on catalytic surface. The technique studies response of the system towards application AC signal of small amplitude. Different AC frequencies were used to carry out measurements and thus got the name of impedance spectroscopy. The system analysis response includes information about structures, their interface and reactions carried out on that interface. [67] The measurement of capacity of the circuit to oppose the flow of charges is called impedance. The important thing about this technique is the ability to separate different processes i.e., charge transfer, mass transfer, ohmic conduction, interfacial charging etc.

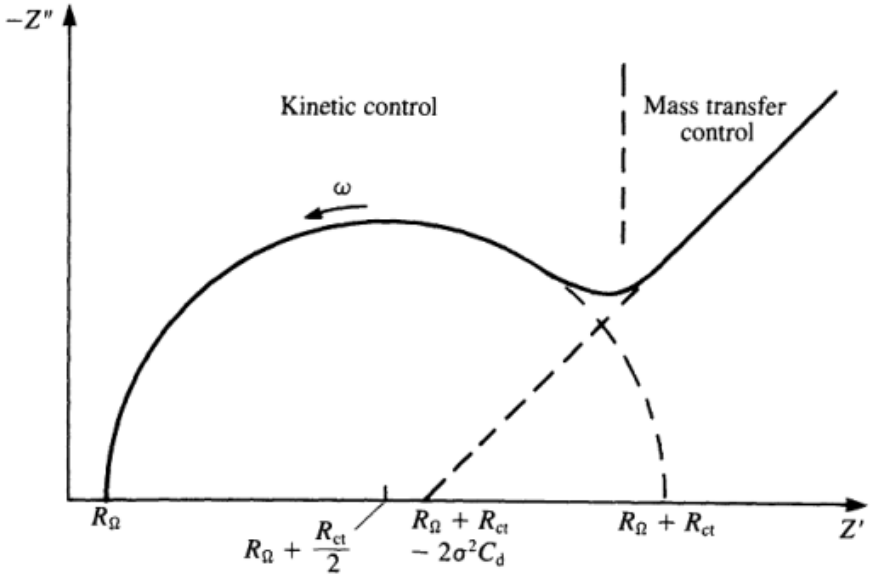

Figure 28: Graphical Representation of EIS

3.6.3 Chronoamperometry

The electrochemical technique used to calculate stability of a catalyst in electrolyte medium is called chronoamperometry. The voltage of working electrode is stopped and current which is produced by faradic process at electrode is monitored with respect to time. This technique is

considered better than other amperometric techniques due to current flowing for longer time intervals.

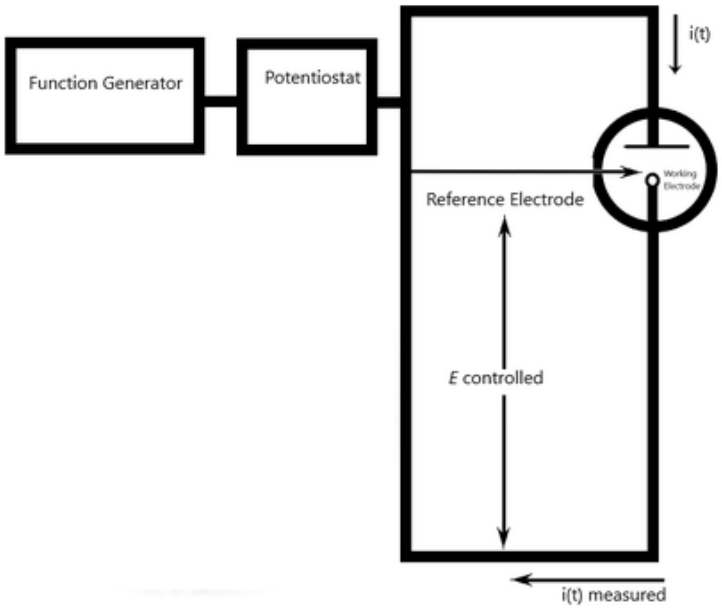

Figure 29: Scheme of chronoamperometry apparatus

The assembly for this process is the same as used in cyclic voltammetry and EIS. The three-electrode system is operated for a prolonged timed for chronoamperometry to find out stability, consistency and sustainability of catalyst [68].

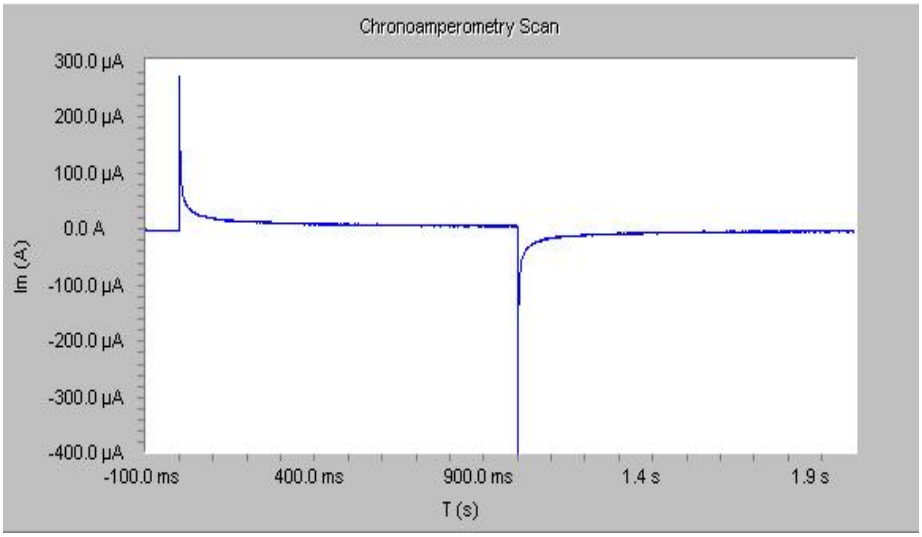

Figure 30: Chronoamperometric graph

Chapter 4

Results and Discussion

4.1 Characterization Techniques

XRD and SEM are used for structural and morphological studies, while FTIR was studied for determining vibrations of functional groups present in catalyst. Electrochemical studies were conducted by performing CV test for current density, EIS for charge transfer resistance and chronoamperometry was done for finding stability and activity of catalyst.

4.1.1 Scanning electron Microscopy

The SEM images of Ni/Fe MOF with its rGO composites shows a variety of different structures which are not seen as perfect geometry, rather a cluster in which Ni/Fe MOF is mixed with its rGO components. The increase in rGO composite is being observed from initial image where there is no sign of rGO to final image where it is prominently shown in the form of sheets.

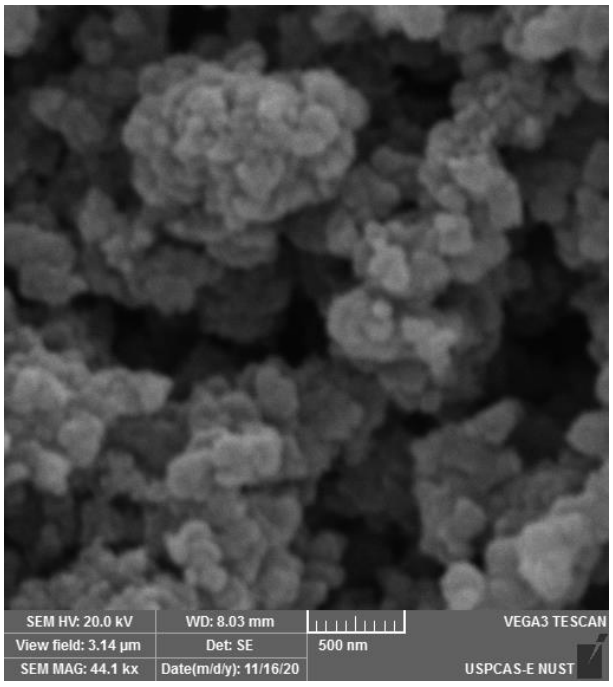

(a)

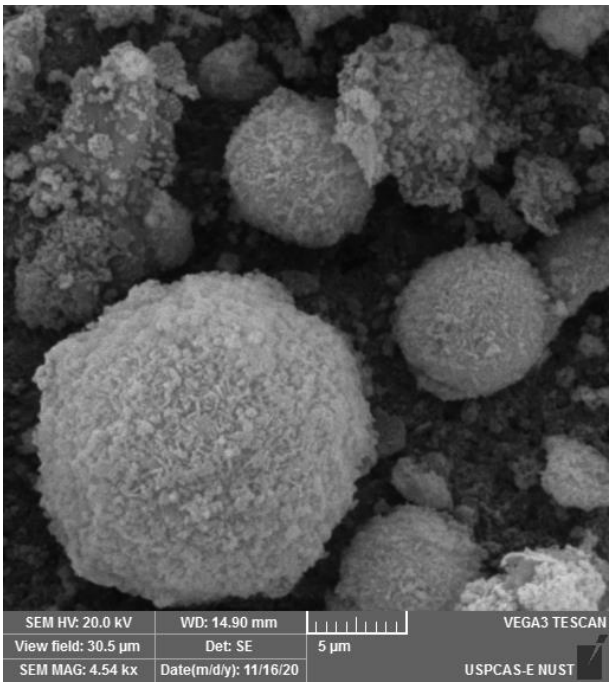

(b)

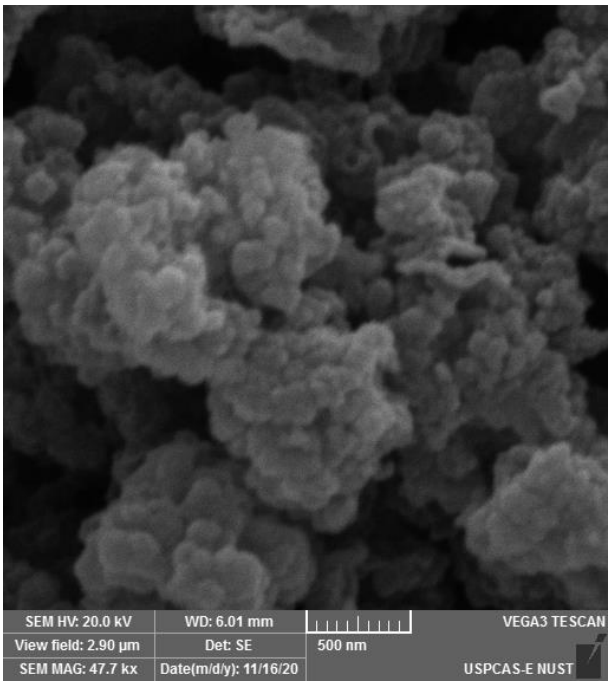

(c)

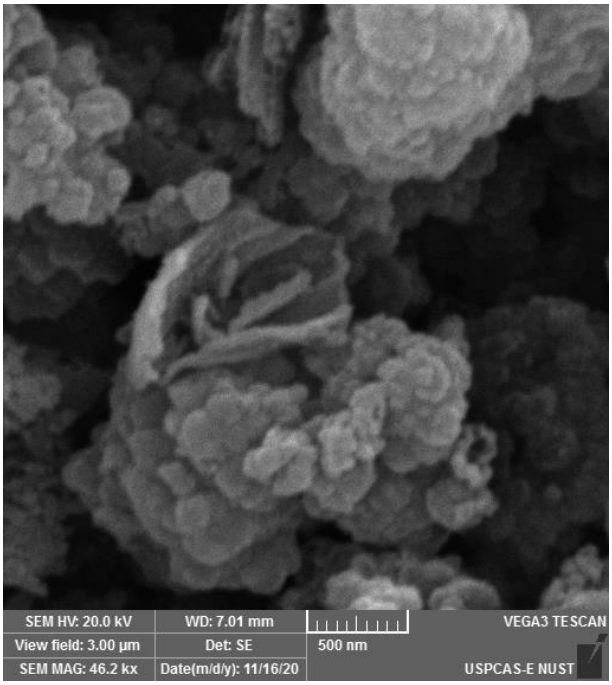

(d)

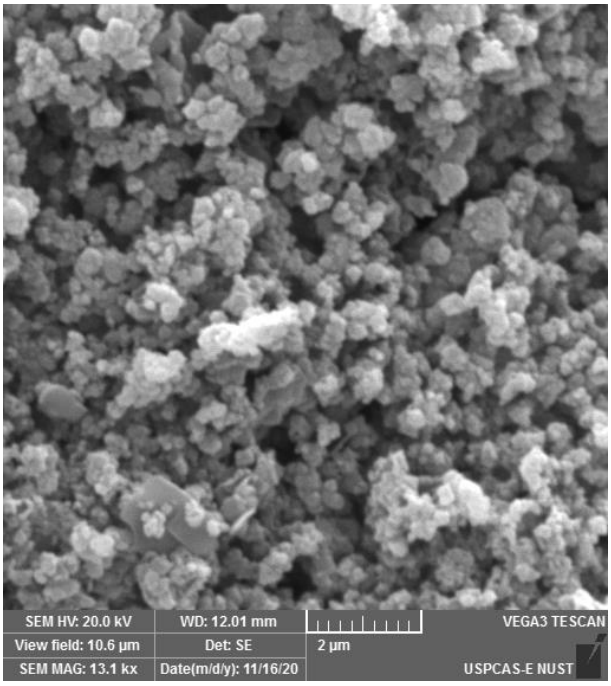

(e)

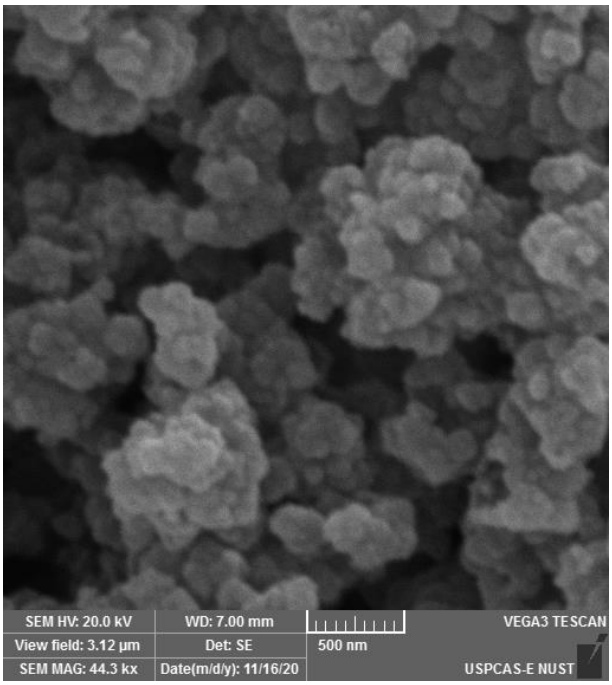

(f)

The MOF structure is clearly shown in SEM images with round shaped agglomerates. The addition of rGO in Ni/Fe MOF also starts to dominate when the increase in weight percent is observed.

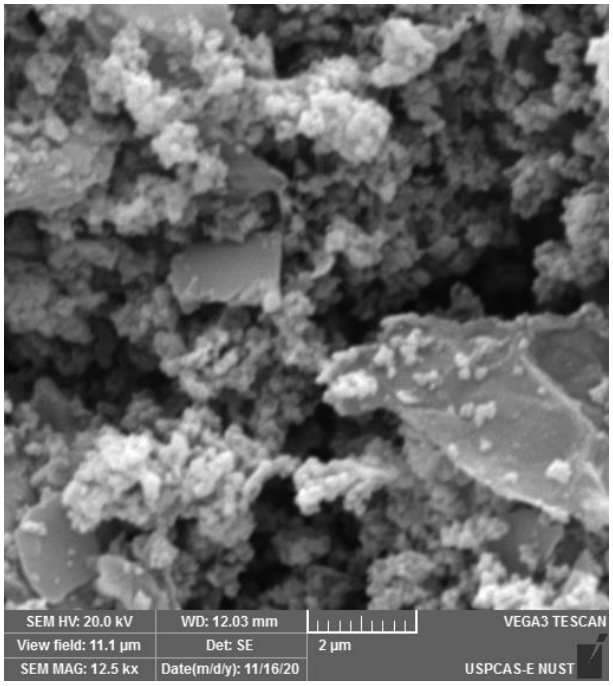

(g)

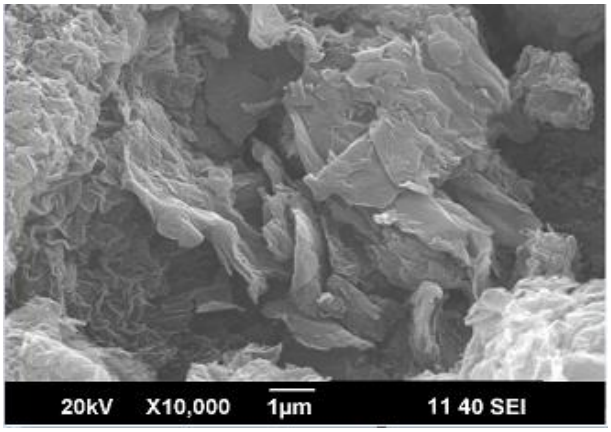

(i)

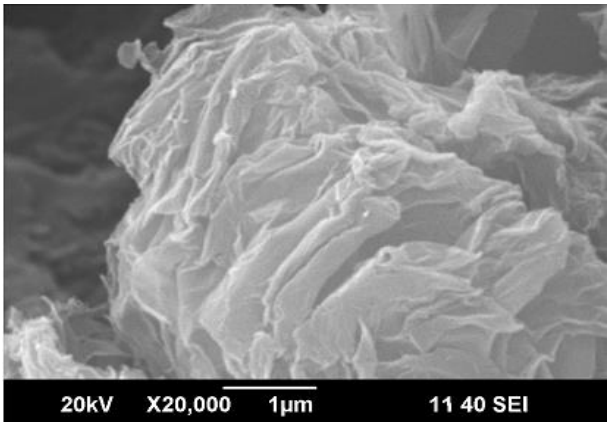

(ii)

Figure 31: SEM images of (a) Ni/Fe MOF (b)1 wt% (c) 2 wt% (d) 3 wt% (e) 4 wt% (f) 5 wt% (g) 8 wt% rGO Ni/Fe MOF and (i) GO (ii) rGO

4.1.2 Energy dispersive X-ray spectroscopy

The elemental analysis on the surface of catalyst is represented by EDX. The analysis of Ni/Fe MOF with its rGO composites given in the representative manner of Ni-Fe MOF, 1, 2, 3, 4, 5 and 8 wt% elaborates the presence of Carbon, Nitrogen, Oxygen, Iron and Nickel on weight% and atomic% basis in table below,

Table 2: Elemental composition of rGO-Ni/Fe composites by weight percentage.

Elements	**weight %**						
	Pure MOF	1	2	3	4	5	8
Carbon	41.97	46.94	46.20	48.75	48.41	45.25	48.89
Nitrogen	11.69	12.53	7.86	10.50	10.21	9.07	9.69
Oxygen	34.11	27.89	36.12	32.87	31.99	32.26	25.44
Iron	3.82	1.48	4.53	4.10	3.93	7.28	7.34
Nickel	8.40	11.16	5.29	3.78	5.46	6.14	8.64

Table 3: Elemental composition of rGO-Ni/Fe composites by atomic percentage.

Elements	**Atomic %**						
	Pure MOF	1	2	3	4	5	8
Carbon	52.24	57.18	56.24	57.95	58.12	56.63	61.55
Nitrogen	12.64	13.58	8.23	10.72	10.59	9.63	10.30
Oxygen	31.92	25.95	33.02	29.36	28.93	30.16	23.90
Iron	1.01	0.39	1.18	1.05	1.02	1.99	2.01
Nickel	2.19	2.90	1.33	0.92	1.35	1.60	2.25

4.1.3 Fourier Transform Infrared Spectroscopy

The FTIR spectrum of characterized material confirmed the functional group vibrations in bimetallic MOF as shown in given figure. The vibration stretching of functional groups in GO represents (C-O) bond at peak of 1212 cm^{1}. The peak at 1648 cm^{-1} (C=C) confirms the structural stretching of alkene group, 1740 cm^{-1} for the stretching of (C=O) carbonyl group and 3756 cm^{-1} for strong vibrations of (O-H) hydroxyl group. FTIR of rGO confirms the absence of hydroxyl group and carbonyl group as there is vibrational stretching peaks. A slight bent at 1650 cm^{-1} represents lattice structure of rGO due to sp^2 hybridization [69].

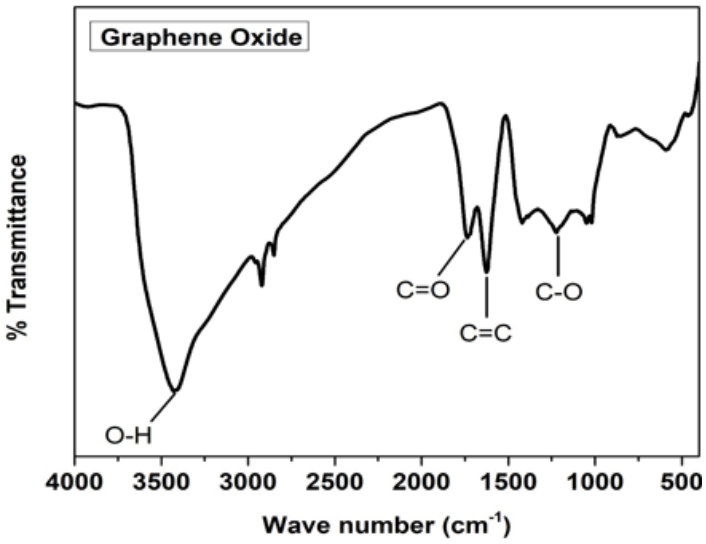

(a)

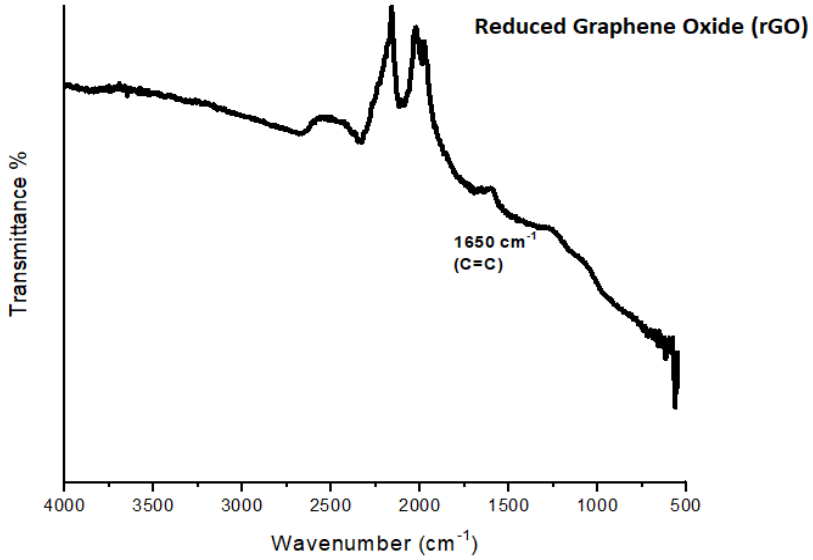

(b)

The presence of various functional groups in Ni/Fe MOF and its composites with rGO were indicated by FTIR analysis. Vibrational bands at 467 cm^{-1} indicate NiO and at 576 cm^{-1} indicate FeO. The band ranging from 1372–1391 cm^{-1} and 1671–1551 cm^{-1} illustrate C=O symmetric and asymmetric stretching. Furthermore, C–H out of plane and in plane bending was observed for DHTA at 1008–748cm-1. All the identification peaks of Ni/Fe MOF with rGO are present in all the prepared composites which also support the successful synthesis of all the prepared series of samples [70].

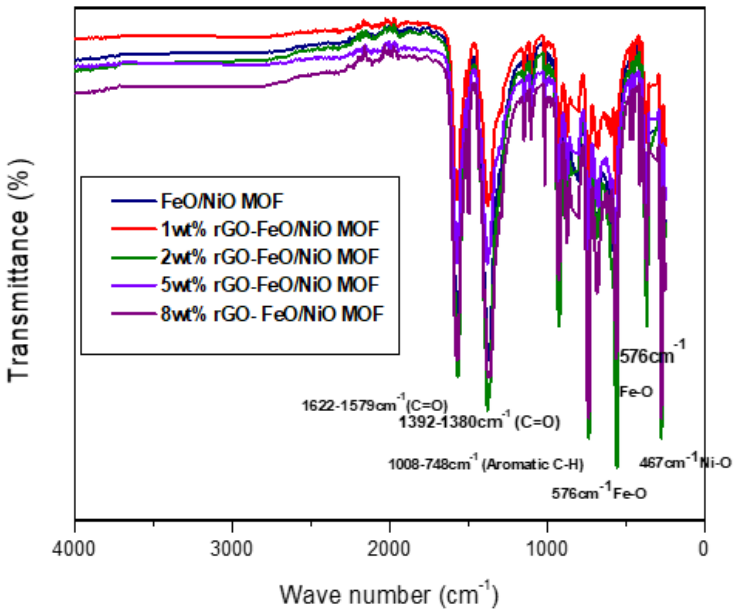

(c)

Figure 32: FTIR of (a) GO (b) rGO (c) Ni/Fe MOF with rGO composites.

4.1.4 X-ray Diffraction

The XRD pattern was of functionalities was examined by figures given below. The GO pattern of XRD matches with reference memory having a sharp intensity peak at angle of 10.3^{o} with (002) lattice plane confirming the reduction of graphite in GO. For the confirmation of rGO, a broad nature of XRD peak at 24.5^{o} with plane sheet of (002) confirms the peak from ICPD library. A short peak of (101) lattice at an angle of 42.7^{o} is present due to some unexfoliated rGO powder [71].

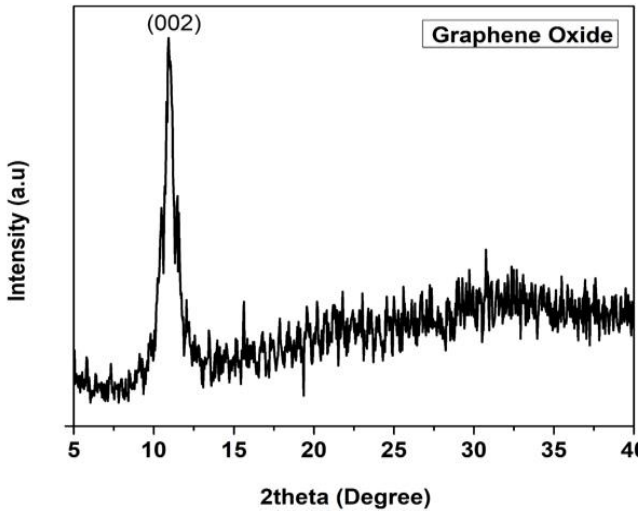

(a)

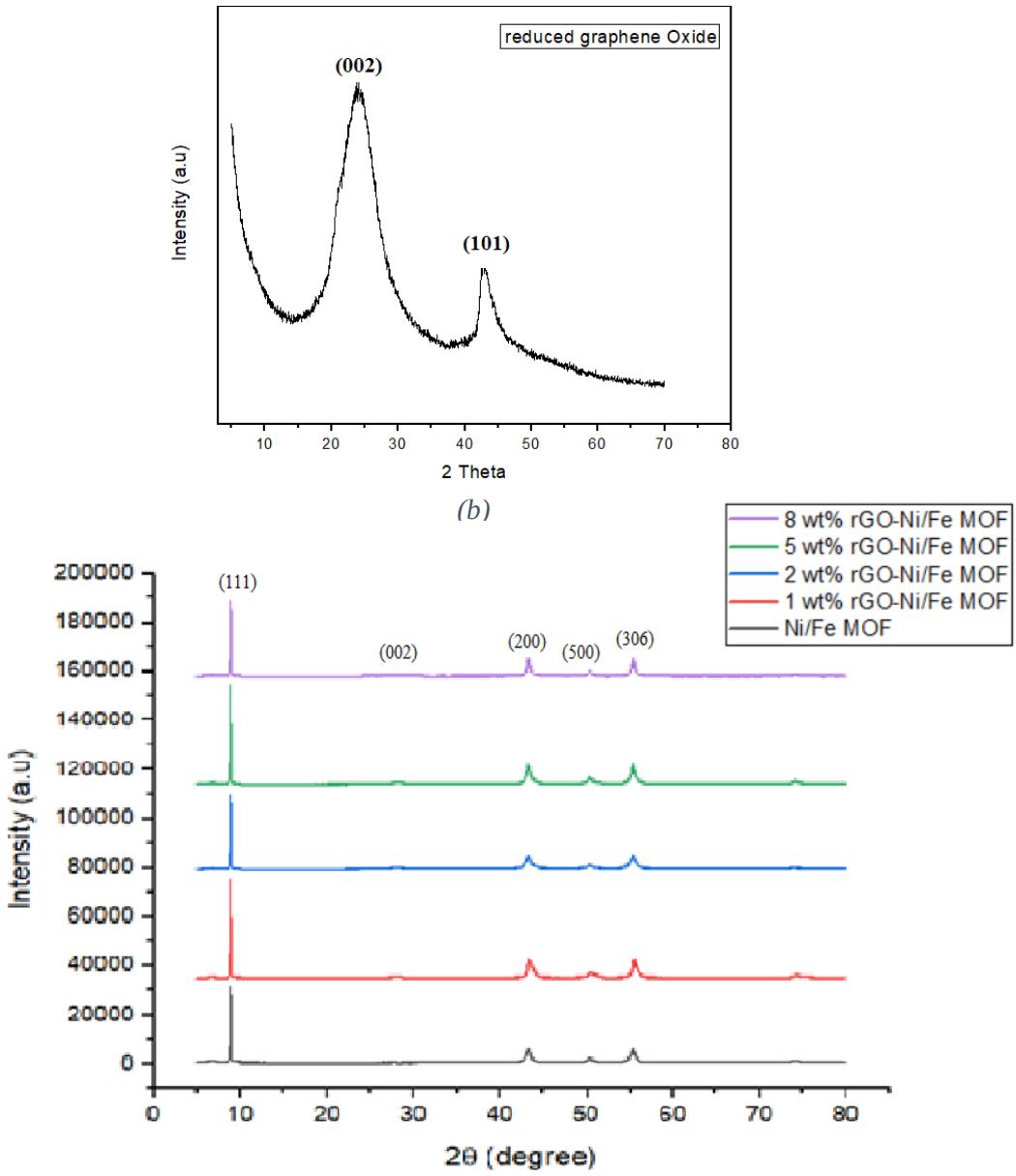

Figure 33: XRD pattern of (a) GO, (b) rGO and (c) Ni/Fe MOF with its rGO composites

The XRD analysis of Ni/Fe MOF with rGO composites represents sharp peaks of crystal lattice. The high intensity peak of 8.9^{o} confirms the synthesis of Ni/Fe MOF. Furthermore, the small peaks at 43.2^{o} correspond to presence of NiO and peaks at 50.4^{o} and 55.2^{o} displays the presence of FeO. All the results confirm the identification of Ni/Fe MOF framework with different lattice surfaces [72].

4.2 Electrochemical Studies

Gamry interface 1010 E is being used for electrochemical studies conducted for the fuel cell. The instrument cover various electrochemical cells specially fuel cell research. High performance CVs, EIS and chronoamperometry can be performed on this instrument.

4.2.1 Cyclic Voltammetry

The electrochemical studies start initially with the testing of bare glassy carbon electrode (GCE) scan. The system consisted of three-neck round bottom flask with three electrodes, i.e.

1. Ag/AgCl as reference electrode
2. GCE as working electrode.
3. Platinum wire as counter electrode.

The flask contains the 3M solution of methanol as fuel and 1M NaOH as supporting electrolyte. The role of NaOH is to provide a sustainable environment for ions transfers between electrodes resulting in an appropriate value of current showing off at different scan rates.

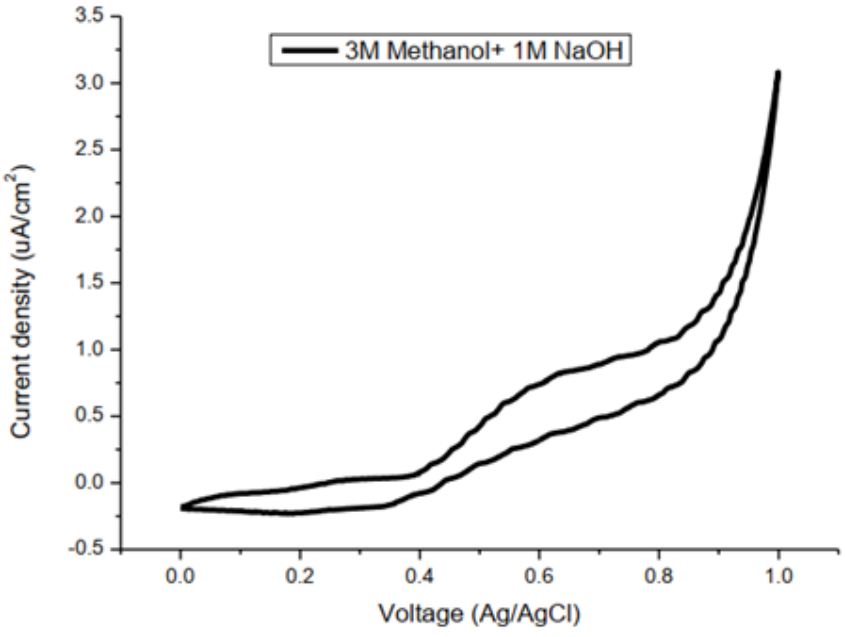

Figure 34: CV scan of bare GCE

The system was modified after conducting the bare GCE test. The GCE was coated with the ink prepared from previous synthesized bimetallic MOF and its composites. Nafion was used as a binder for the ink. Different concentrations of inks were prepared for catalyst and their composites for understanding the performance of catalyst for methanol oxidation.

4.2.2 Effect of Reduced Graphene Oxide

The same process of ink preparation was carried out with Ni/Fe MOF with its rGO composites. As reduced graphene oxide possess supportive qualities of having high charge conductivity, large surface area, durability and electron dispersity, it acts as a supporting material as well as current enhancer when combined with Ni/Fe MOF. The resultant performance of catalyst makes it efficient and promising material for methanol oxidation. Previously done with MOF concentration, the concentration of rGO along with Ni/Fe MOF is also varied to find out optimum quantity of catalyst for methanol oxidation. The composites were synthesized with different weight percentages of rGO i.e., 1, 2, 3, 4, 5 and 8 wt% rGO – Ni/Fe MOF. About 2 mg of catalyst was used for ink preparation with 20 µl nafion as binder and 100 µl of ethanol as solvent. A thin layer of ink is attached with glassy carbon electrode and dipped in 3M CH_3OH solution for oxidation. The graph shows the comparison between current densities of Ni/Fe MOF with different weight ratios of rGO [73].

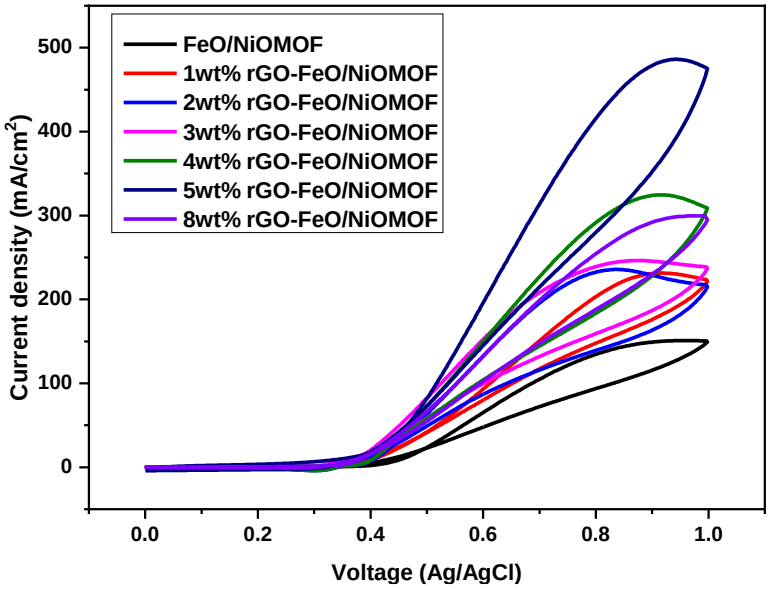

Figure 35: Cyclic voltammograms of Ni/Fe MOF with rGO composites.

The scan rate was set about 50 mV/sec with each composite given three to five cycles of scan. Gradual change of current was observed in 3M methanol solution with 1M NaOH. As the results are compared, it is clearly visible from the graph that incorporation of rGO enhances the current density. Furthermore, by increasing the ratio of rGO in composites the current densities also increase. The result showed the highest current density of 5 wt% Ni/Fe MOF of about 482 mA/cm^2. Other composites gave the current densities i.e., 232, 238, 245 and 323 mA/cm^2 respectively for composites of 1, 2, 3 and 4 wt%. It is important to note that current density of 8 wt% rGO with Ni/Fe MOF is 300 mA/cm^2, which is substantially lower than that of 5 wt%. This behavior could be due to composite dominating the bimetallic MOF in activity. As a result, more surface area is covered by rGO and less active sites are available for methanol oxidation. As for the pure Ni/Fe MOF, the current density was found to be 153 mA/cm^2 which indicated that pure Ni/Fe MOF is bad conductor of charge and requires electroactive material for conduction of electrons. Since the purpose of Ni/Fe MOF is to provide active sites for methanol to oxidize, reduced graphene oxide performs the task of electron conduction. From all the composite of Ni/Fe MOF with rGO, the best activity was shown by 5 wt% rGO with Ni/Fe MOF. Reduced graphene oxide was preferred upon graphene oxide due to its high conductivity, stability, and thin film composition with MOF which makes it compatible with given bimetallic MOF [49].

4.2.3 Effect of different scan rates

The variation in weight percentage of reduced graphene oxide with Ni/Fe MOF is followed by studying the variation in scan rate given for methanol oxidation. Scan rate is basically the rate of voltage change in experiment. The main purpose of studying the behavior of scan rate is to know how fast the applied voltage is scanned. The faster scans lead to decrease in diffusion of methanol over the catalyst, thus adsorption behavior is dominant. As a result, higher peaks of current densities are observed when increasing potentials.

In previous experiment, the scan rates were fixed at 50 mV/sec to observe the current densities related to different wt% of composites. This experiment was performed on different scan rates i.e., 50, 100, 150 and 200 mV/sec for all given weight percentages of MOF with composites [74]. All the tests were conducted under concentration of 3M CH_3OH solution supported by alkaline solution of 1M NaOH.

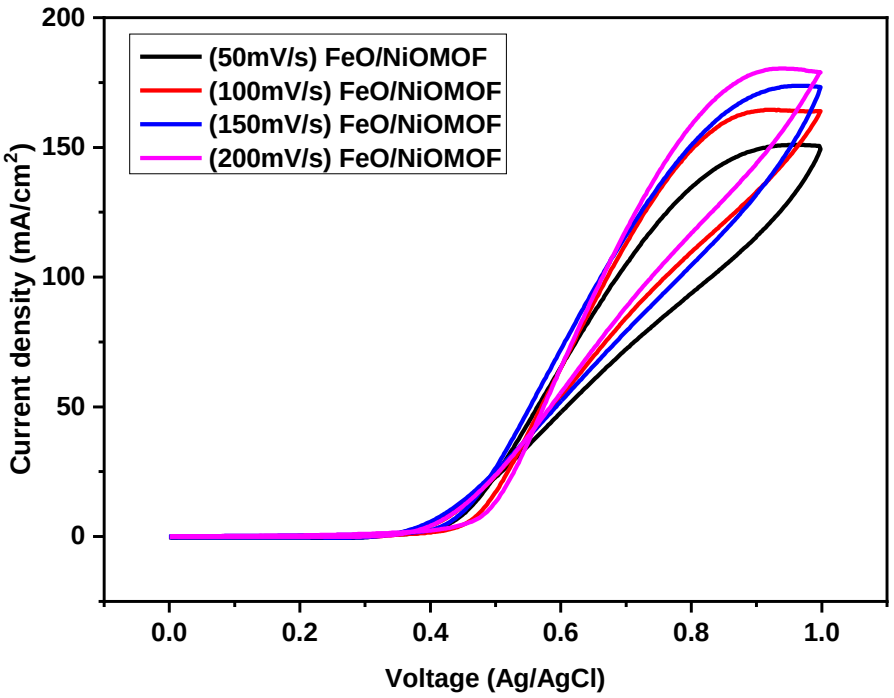

(a)

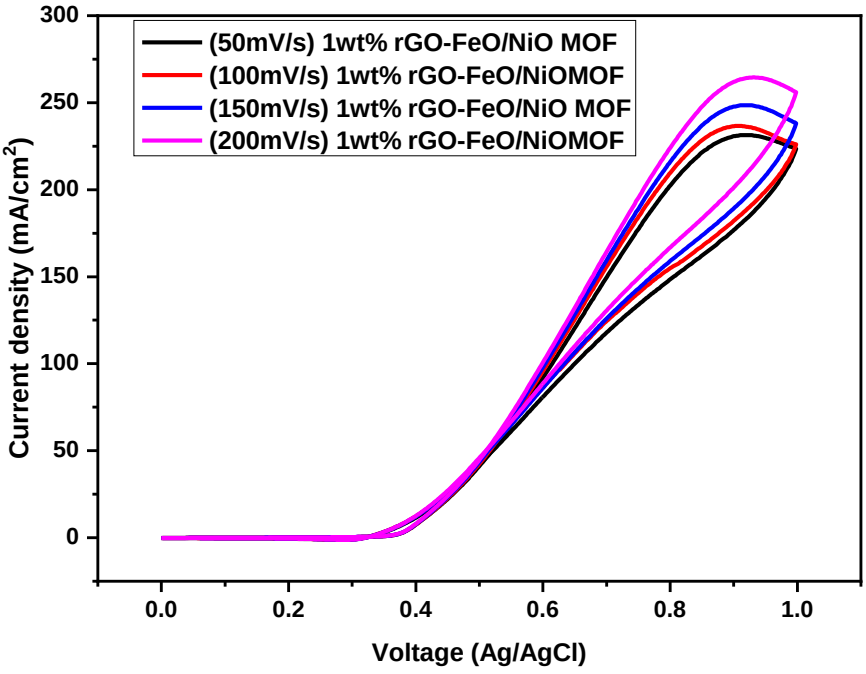

(b)

The increase in scan rate of system rapidly induces the high peaks of current which is evident from the graphical images.

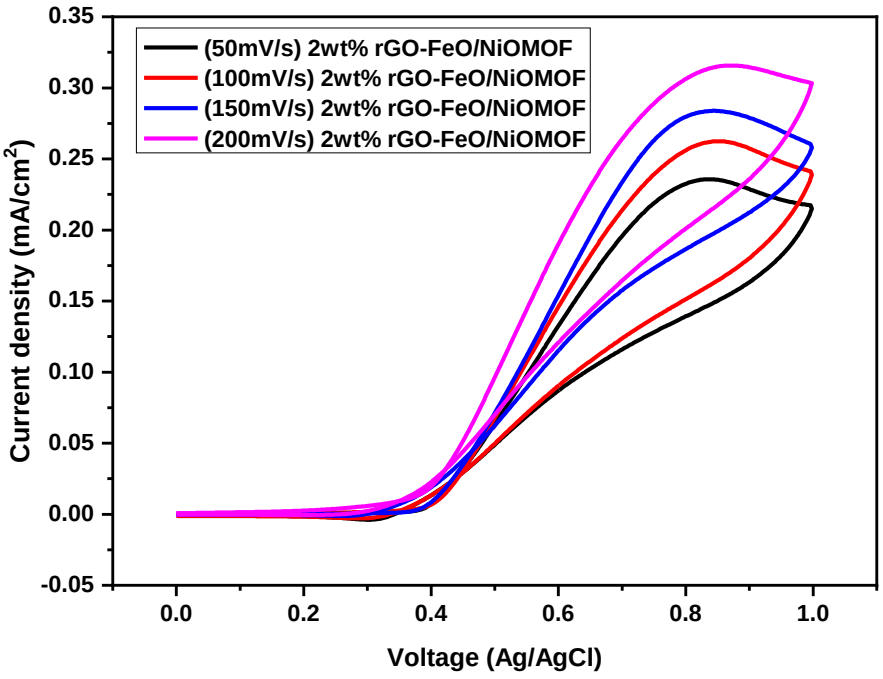

(c)

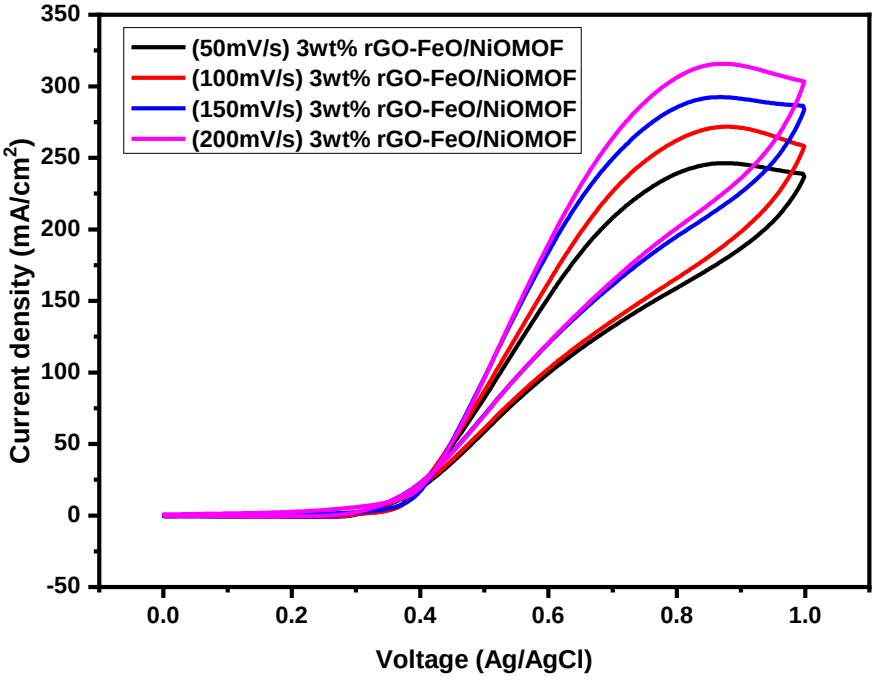

(d)

The following pattern follows for all the given composites and they all display similar behavior. The fact that rGO is also incorporated with Ni/Fe MOF helps in enhancing the current density of the system.

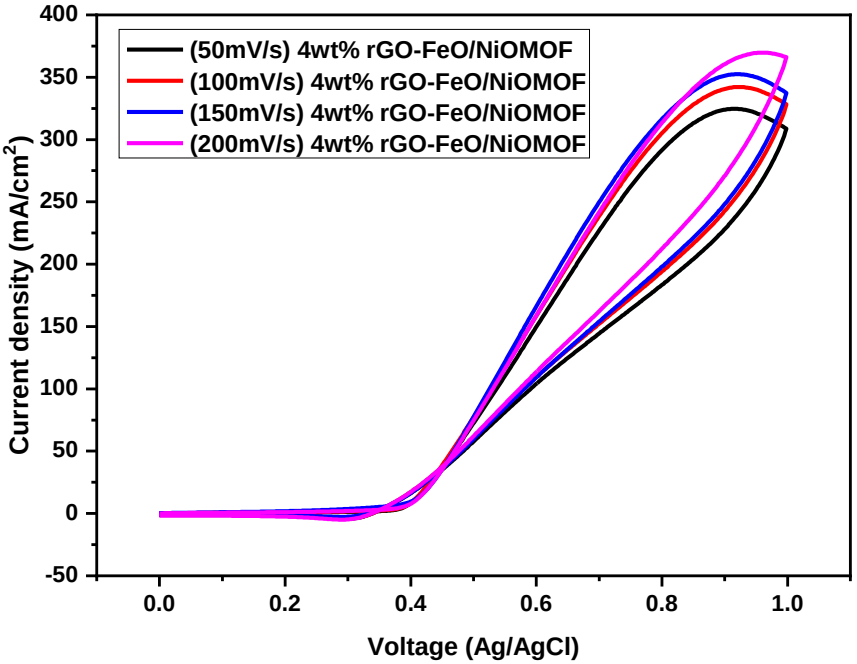

(e)

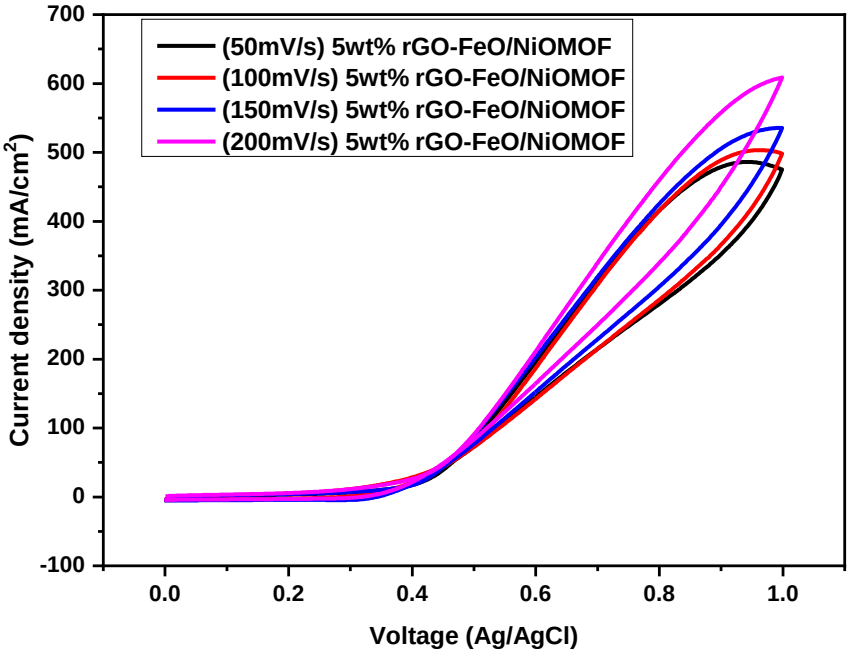

(f)

The scan rate was not exceeded above 200 mV/sec because of the reason i.e., rate of reaction proceeds fast and there will be little to no time for the reaction to take place due to the slow kinetics of system.

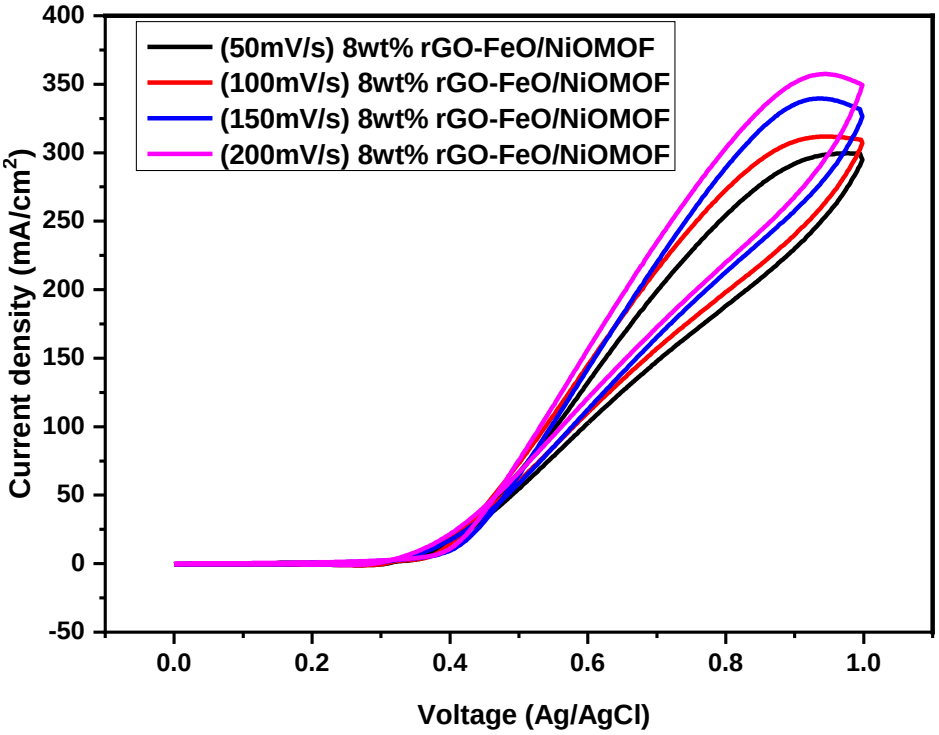

(g)

Figure 36: Cyclic Voltammogram of (a) Ni/Fe MOF with composites (b) 1 , (c) 2 , (d) 3 , (e) 4 , (f) 5 , (g) 8 wt % rGO at scan rates of 500, 100, 150, 200 mV/sec in 1 M NaOH and 3 M CH_3OH.

For oxidation to take place, methanol requires enough time for diffusion from the bulk of solution towards active sites of catalyst. The catalyst then oxidizes methanol to aldehyde, acetic acid and carbon dioxide while transferring ions through membrane and electrons through the circuit. By increasing the scan rate there would be less time for methanol diffusion and no current peak will occur.

On the other hand, the trend of scan rate along with increase in current density indicates the implication of Randles-Sevick principle. The reason behind this is increase in concentration gradient. Due to increased concentration, higher diffusion rates of analyte are observed from bulk of solution to electrode surface. On surface of electrode, oxidation of methanol takes place and it converts into formaldehyde, formic acid and carbon dioxide and water. The ions transfer from bulk

of solution towards working electrode where they oxidize, giving charge to electrode which travels through circuit to give electrons as current.

4.2.4 Electrochemical Impedance Spectroscopy

Generally known as AC impedance, electrochemical impedance spectroscopy studies reactions carried out in potentiometer, interface responses and resistance due to analyte and electrode circuit. Ohmic law describes resistance as important factor in governing the flow of current. Impedance or resistance is a hinderance to flow of current in any circuit. The apparatus uses the same design of potentiometric cell which includes three electrode system. Initially modified glassy carbon electrode was tested in 3M CH_3OH supported by 1M NaOH solution. The resistance between working and reference electrode plays an importance role in charge transfer with bulk of solution resisting ions flow [49]. For the graphical representation of EIS, Nyquist plot and Bode plot are used. For Nyquist plot, real and imaginary resistance are plotted on x and y-axis respectively.

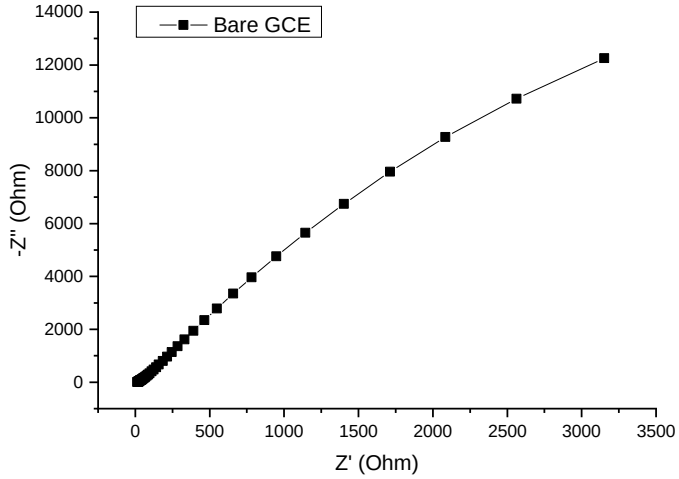

Figure 37: Nyquist plot of bare GCE in 1M NaOH and 3M CH_3OH solution.

Nyquist plot for given system shows difference in impedance when bare GCE electrode was compared with different concentrations of Ni/Fe MOF. In case of increase in concentration of Ni/Fe MOF, the ions diffuse easily on to the electrode surface and easily oxidizes. The resistance occurs in charge transfer. Figure 38, depicts the graphical representation of this,

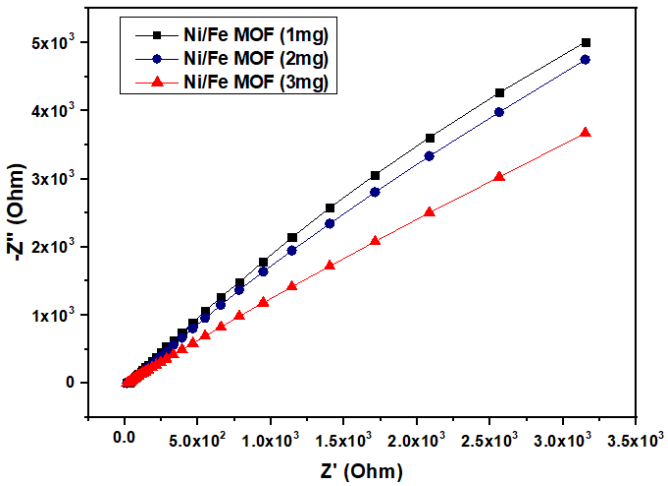

Figure 38: Nyquist plot of Ni/Fe MOF at different concentration in 3M CH_3OH and 1M NaOH solution

For the composites of rGO with Ni/Fe MOF, impedance decreases significantly. The graph show that by increasing the concentration of rGO in Ni/Fe MOF, the resistance of the system decreases. The is due to higher charge transfer of reduced graphene oxide and increased surface area for the catalyst to absorb and diffuse ions. As the figure represents, pure catalyst shows high resistance but by mixing it with rGO composites, the resistance decreases. The best favorable behavior was shown by 8 wt% rGO-Ni/Fe MOF due to high surface area and charge transfer capacity. But 8 wt% composite shows low current density due to high coverage of sites than catalyst. This inhibits methanol to adsorb on active sites of catalyst showing low current density.

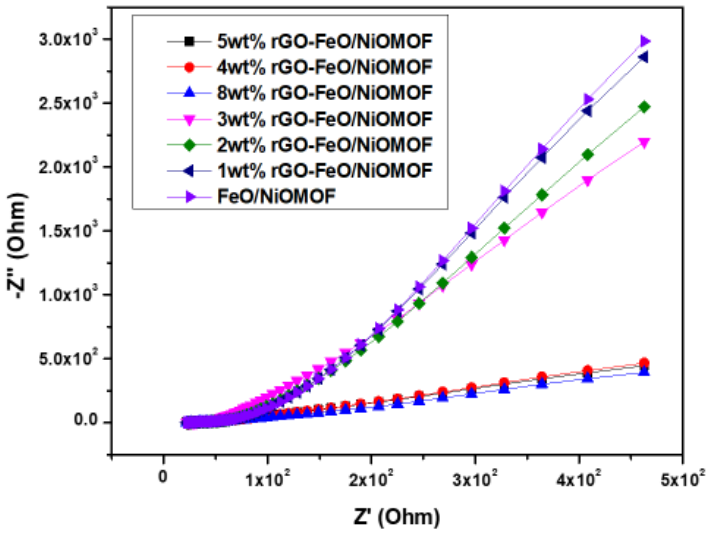

Figure 39: Comparative plot of bare GCE, Ni/Fe MOF with rGO composite

Figure 40 shows linear relation of square root of scan rates vs peak current densities for Ni/Fe MOF with its rGO composites. The plots show linear the domination of diffusion-controlled process when increasing the scan rates for methanol oxidation [75]. From the graph, the values of transfer coefficient and diffusion coefficient (D) can be calculated.

Diffusion coefficient is calculated by Randles-Sevcik equation:

$$i_p = (2.99 \times 10^5)\, n\, (\alpha\, n_a)^{\frac{1}{2}}\, A\, C\, D^{\frac{1}{2}}\, v^{\frac{1}{2}}$$

Where,

i_p = peak current density

A = Area of electrode

n = No. of electrons transferred

V = Scan rate

α = Transfer coefficient

C = Concentration

n_a = electrons in RDS

D = Diffusion coefficient

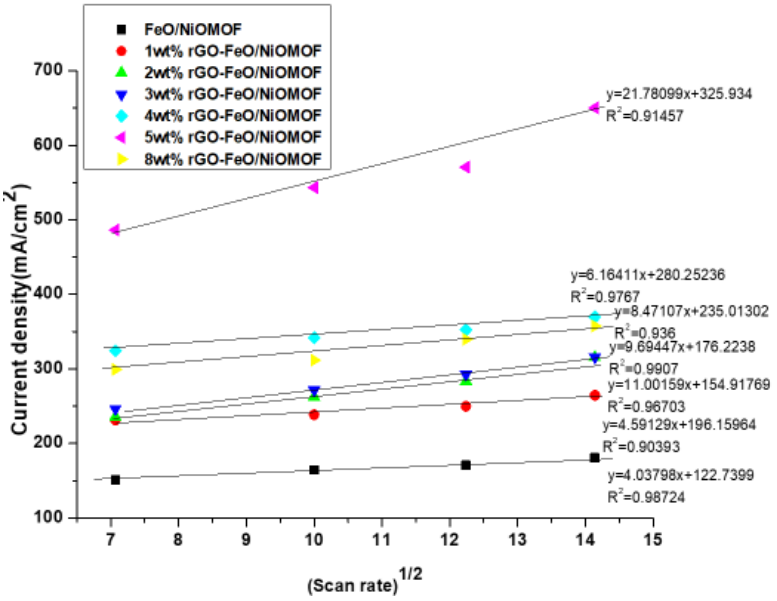

Figure 40: Plots of square roots against peak current densities of Ni/Fe MOF with its composites

Table 4: Diffusion coefficients of Ni/Fe MOF and (1 wt%, 2 wt%, 3 wt%, 4 wt%, 5 wt%, 8 wt%) rGO with Ni/Fe MOF

Catalyst	Diffusion Coefficient
Ni/Fe MOF	3.23×10^{-7}
1 wt% Ni/Fe-rGO MOF	1.45×10^{-6}
2 wt% Ni/Fe-rGO MOF	4.85×10^{-6}
3 wt% Ni/Fe-rGO MOF	4.92×10^{-6}
4 wt% Ni/Fe-rGO MOF	7.67×10^{-6}
5 wt% Ni/Fe-rGO MOF	1.47×10^{-5}
8 wt% Ni/Fe-rGO MOF	3.35×10^{-6}

4.2.5 Chronoamperometry

Usually, a way to find diffusion of analyte on catalyst, chronoamperometry refers to the relation of current dependent upon time. By applying step voltage to the working electrode, the current of that electrode is calculated as time function. As the fuel diffuses from bulk solution towards the electrode, the current fluctuates showing the current-time relation of a diffusion-controlled process for working electrode. For time up to 36000 seconds, the stability of synthesized catalyst was also measured by using the electrochemical setup of working, reference and counter electrode. The solution to be oxidized is mixture of 3M CH_3OH with 1M NaOH as supporting electrolyte. The given potential for chronoamperometry was 0.9 V. The figure below shows the resultant curves of chronoamperometry for all prepared samples. Furthermore, these curves guide about the comparison between pure Ni/Fe MOF with its rGO composites of (1, 2, 3, 4, 5 and 8 wt%) for stability of catalyst.

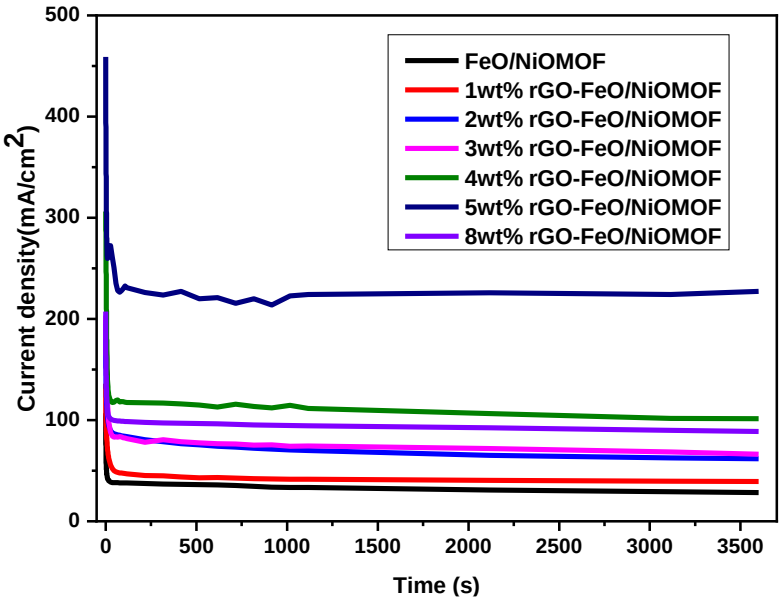

Figure 41: Chronoamperometric plots for Ni/Fe MOF and with its rGO composites at scan rate of 50 mV/sec

The current density of 5 wt% rGO with Ni/Fe MOF shows stabilizes on 230 mA/cm^2. Similarly, Ni/Fe MOF shows about 37 mA/cm^2. All the remaining composites show the current density of 42 mA/cm^2, 75 mA/cm^2, 87 mA/cm^2, 115 mA/cm^2 and 100 mA/cm^2 for 1, 2, 3, 4 and 8 wt% rGO composites respectively. Figure show how much the catalyst was stabilized for given time of 3600 sec while performing methanol oxidation reaction.

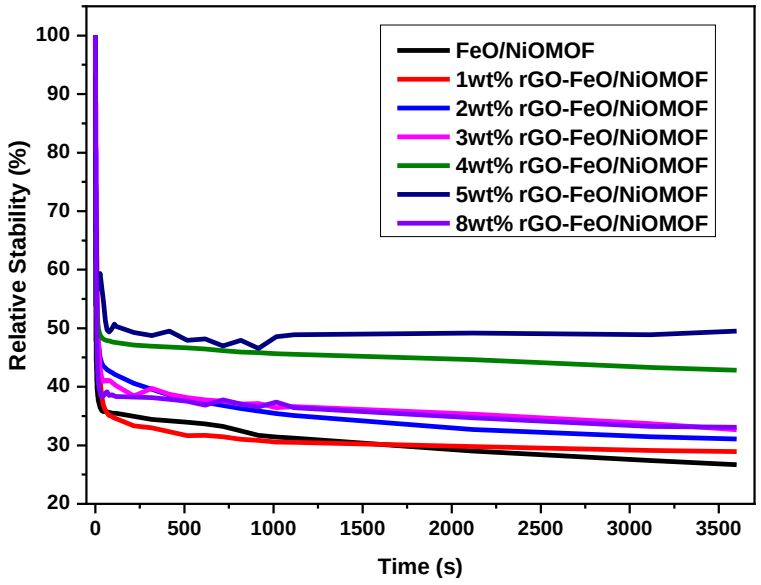

Figure 42: Chronoamperometric plot for stability of a catalyst for 3600 sec in 3M CH_3OH and1M NaOH solution

Among all the given catalysts, 5 wt% rGO wit Ni/Fe MOF shows highest stability of 55%. Initially, a sharp dropdown was noticed in beginning of reaction for 60 sec. Afterwards, all the catalysts stabilized in given conditions. This may be due to less diffusion of Methanol or intermediate formation like carbon monoxide which hinders the reaction. For set potential of 0.9 V for 3600 seconds, Ni/Fe MOF shows 27% stability, 1 wt% shows 30% stability, 2 wt% shows 35 % stability, 3 wt% shows 38% stability, 4 wt% shows 45% stability and 8 wt% shows about 37% stability.

4.2.6 Tafel Plot

Tafel plots are a way to represent reaction kinetics of the catalyst present in the system. It is a plot between over potential required to increase the reaction ration by factor of 10. It can also be use as polarization technique for measurement of corrosion rates as they also represent redox reactions [76]. Thermodynamic and kinetics of reaction can be described simply with the help of tafel extrapolation. In figure 43, all the composites of rGO-Ni/Fe MOF are plotted on tafel graph by comparing the overpotential and current density. For the ideal case scenario, Pt shows 0.0 V as overpotential for methanol oxidation. The catalyst performed on low potentials of 0.4 V with ideal results of current densities as voltage increases. The reason could be optimum amount of rGO available for adsorbing the reactant by providing large surface area, stability and facilitating the oxidation of methanol through charge transfer capacity [77].

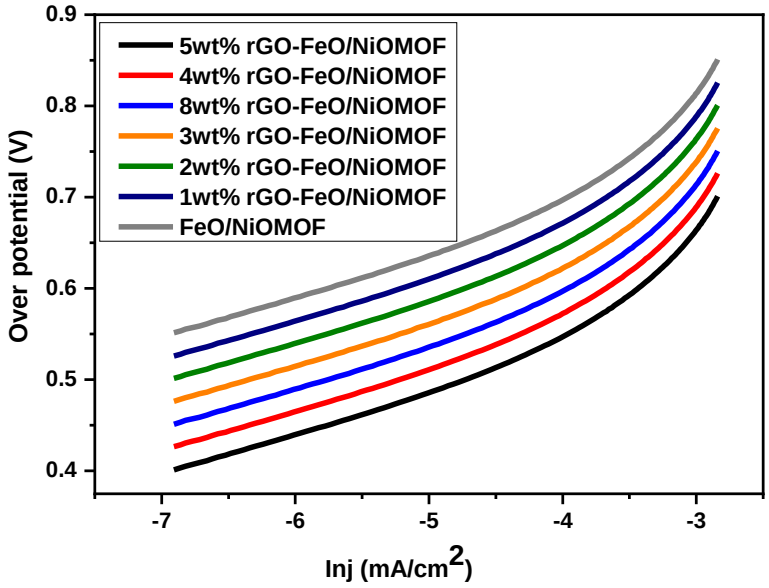

Figure 43: Tafel plots of Ni/Fe MOF with its rGO composites in 1M NaOH and 3M CH_3OH solution.

4.2.7 Comparison with Literature

A thorough comparison of catalyst used previously in methanol oxidation reaction have been carried out with present work. Different literatures have been studies and parameters such as scan rate, current densities, peak potential and methanol concentration have been compared. NiCo/NiO-CoO/NPCC/GCE based bimetallic catalyst showed current density of 178 mA/cm^2 ant peak potential of 0.61 v potential. 5 wt% rGO/Co MOF showed peak current of 29.1 mA/cm^2 at expense of 0.1 V. Incorporation of rGO enhanced the surface area for diffusion of catalyst along with current densities. Furthermore, the bimetallic MOF incorporation in methanol oxidation reaction enhances the catalytic activity to absorb incoming ions and oxidize them to give current. Ni/Cu MOF with 5% rGO composite show remarkable current density of 437.28 mA/cm^2 at 0.9 V peak potential. The reported results in this paper showed promising results in further progress in DMFCs. The given Ni/Fe MOF shows charge density of 153 mA/cm^2 with peak potential of 0.8 V. With incorporation of rGO in Ni/Fe MOF, its tendency to diffuse ions and supplying current increases. The highest of current densities was shown by 5 wt% rGO-Ni/Fe MOF of about 482 mA/cm^2.

Table 5: Comparison between different literatures and present work

	Author	**Catalyst**	**MeOH Conc. (M)**	**Scan rate (mV/sec)**	**Current density**	**References**
1	R. Ganesan et al.	Pt/W-C	1	50	185 mAcm^{-2}	[78]
2	Rimsha et al.	GO/Co-MOF	3	50	29 mAcm^{-2}	[49]
3	T. Noor et al.	5 wt% rGO-Ni/Cu MOF	3	50	437 mAcm^{-2}	[46]
4	Yang et al.	Pt/Ni CNC	0.5	100	696 mAmg^{-1}	[79]
5	Rezaee et al.	NiCo-NPCC	0.5	50	178 mAcm^{-2}	[80]
6	This work	Ni/Fe MOF	3	50	153 mAcm^{-2}	
7	This work	5 wt% rGO-Ni/Fe MOF	3	50	482 mAcm^{-2}	

Conclusion

Ni/Fe MOF was synthesized by hydrothermal method using two different linkers. As a supporting element for catalyst and current enhancer, reduced graphene oxide (rGO) was also synthesized via improved Hummer's process. Composites of rGO with Ni/Fe MOF of 1, 2, 3, 4, 5 and 8 wt% were made for electrochemical testing for methanol oxidation for DMFC. All the samples were characterized by XRD, FTIR and SEM.

Electrochemical properties of bimetallic MOF were studies via electrochemical impedance spectroscopy, cyclic voltammetry and chronoamperometry techniques. A setup of three electrode system with, platinum as counter electrode, Ag/AgCl as reference electrode and glassy carbon as working electrode was utilized in electrochemical testing. For all the electrochemical test, the scan rate was about 50 mV/sec with electrolyte of 1 M NaOH and 3 M CH_3OH solution.

GCE and Pt wire were tested first desired electrochemical results. Afterward, CV was performed on all composites of rGO and Ni/Fe MOF. With the increment in wt% of rGO, the current density starts increasing with maximum of 482 mA/cm^2. 8 wt% rGO with Ni/Fe MOF shows slightly less conductivity and compared to 5 wt%. The resistance to charge transfer is calculated be EIS, which show minimum resistance for 5 wt% rGO-Ni/Fe MOF. For finding out stability of catalyst, chronoamperometry test was conducted which also concluded the best results for 5 wt% rGO-Ni/Fe MOF over period of 3600 seconds. rGO provides stability to the catalyst, increases the current density and provide high surface area for reactants. On the other hand, Ni/Fe MOF oxidizes methanol to its final component i.e., CO_2 while suppressing CO poisoning.

The following results were also matched by different literatures having effective results as compared to noble metals. With simple technique of synthesis, Ni/Fe MOF appeared to be promising catalyst for the oxidation of methanol in DMFC and opens the way ahead for more research in application of non-noble metal as catalyst for methanol oxidation in DMFC.

The end result shows that synthesized catalyst is promising for oxidation of methanol and could be applied systematically in DMFC as catalyst.

Future Recommendations

- Inclusion of any noble metal such as Pt, Pd, Ru in bimetallic MOF to find out extent of methanol oxidation reaction.
- The Ni/Fe MOF could also be studied for oxygen evolution reaction (OER) for future purposes
- Temperature variations can also be test on composite of rGO-Ni/Fe MOF for better understanding of operating conditions.
- The catalyst can also be studied for oxidation of other organic fuel like ethanol, propanol, aldehydes etc. for high energy density.

References

[1] J. Wang, H. Wang, and Y.Fan, *Techno-economic challenges of fuel cell commercialization.* Engineering, 2018. **4**(3): p. 352-360.

[2] S. Shafiee and E. Topal, *When will fossil fuel reserves be diminished?* Energy policy, 2009. **37**(1): p. 181-189.

[3] J. Jurasz, F. Canales, A. Kies, M. Guezgouz, and A. Beluco, *A review on the complementarity of renewable energy sources: Concept, metrics, application and future research directions.* Solar energy, 2020. **195**: p. 703-724.

[4] M. Secanell, J. Wishart, and P. Dobson, *Computational design and optimization of fuel cells and fuel cell systems: A review.* Journal of Power Sources, 2011. **196**(8): p. 3690-3704.

[5] O. Z. Sharaf and M. F. Orhan, *An overview of fuel cell technology: Fundamentals and applications.* Renewable and Sustainable Energy Reviews, 2014. **32**: p. 810-853.

[6] N. Sammes, R. Bove, and K. Stahl, *Phosphoric acid fuel cells: Fundamentals and applications.* Current Opinion in Solid State and Materials Science, 2004. **8**(5): p. 372-378.

[7] G. McLean, T. Niet, S. Prince-Richard, and N. Djilali, *An assessment of alkaline fuel cell technology.* International Journal of Hydrogen Energy, 2002. **27**(5): p. 507-526.

[8] A. L. Dicks, *Molten carbonate fuel cells.* Current Opinion in Solid State Materials Science, 2004. **8**(5): p. 379-383.

[9] N. J. Cherepy, R. Krueger, K. J. Fiet, A. F. Jankowski, and J. F. Cooper, *Direct conversion of carbon fuels in a molten carbonate fuel cell.* Journal of the Electrochemical Society, 2004. **152**(1): p. 80-87.

[10] A. B. Stambouli and E. Traversa, *Solid oxide fuel cells (SOFCs): a review of an environmentally clean and efficient source of energy.* Renewable and Sustainable Energy Reviews, 2002. **6**(5): p. 433-455.

[11] Y. Wang, K. S. Chen, J. Mishler, S. C. Cho, and X. C. Adroher, *A review of polymer electrolyte membrane fuel cells: Technology, applications, and needs on fundamental research.* Applied Energy, 2011. **88**(4): p. 981-1007.

[12] B. Smitha, S. Sridhar, and A. Khan, *Solid polymer electrolyte membranes for fuel cell applications—a review*. Journal of Membrane Science, 2005. **259**(1-2): p. 10-26.

[13] S. Sharma and B. G. Pollet, *Support materials for PEMFC and DMFC electrocatalysts—a review.* Journal of Power Sources, 2012. **208**: p. 96-119.

[14] X. Lü, Y. Qu, Y. Wang, C. Qin, and G. Liu, *A comprehensive review on hybrid power system for PEMFC-HEV: Issues and strategies*. Energy Conversion and Management, 2018. **171**: p. 1273-1291.

[15] Y.-H. Liu, B. Yi, Z.-G. Shao, L. Wang, D. Xing, and H. Zhang, *Pt/CNTs-Nafion reinforced and self-humidifying composite membrane for PEMFC applications.* Journal of Power Sources, 2007. **163**(2): p. 807-813.

[16] S. K. Kamarudin, F. Achmad, and W. R. W. Daud, *Overview on the application of direct methanol fuel cell (DMFC) for portable electronic devices.* International Journal of hydrogen energy, 2009. **34**(16): p. 6902-6916.

[17] S. J. Peighambardoust, S. Rowshanzamir, and M. Amjadi, *Review of the proton exchange membranes for fuel cell applications.* International Journal of Hydrogen Energy, 2010. **35**(17): p. 9349-9384.

[18] L. E. Kreno, K. Leong, O. K. Farha, M. Allendorf, R. P. Van Duyne, and J. T. Hupp, *Metal–organic framework materials as chemical sensors.* Chemical reviews, 2012. **112**(2): p. 1105-1125.

[19] H.-C. Zhou, J. R. Long, and O. M. Yaghi, *Introduction to metal–organic frameworks*. 2012, ACS Publications: Chemical Reviews. p. 673-674.

[20] H. Li, M. Eddaoudi, M. O'Keeffe, and O. M. Yaghi, *Design and synthesis of an exceptionally stable and highly porous metal-organic framework.* Nature, 1999. **402**(6759): p. 276-279.

[21] W. Liang, R. Babarao, and D. M. D'Alessandro, *Microwave-Assisted Solvothermal Synthesis and Optical Properties of Tagged MIL-140A Metal–Organic Frameworks.* Inorganic Chemistry, 2013. **52**(22): p. 12878-12880.

[22] T. V. de Medeiros, J. Manioudakis, F. Noun, J.-R. Macairan, F. Victoria, and R. Naccache, *Microwave-assisted synthesis of carbon dots and their applications.* Journal of Materials Chemistry C, 2019. **7**(24): p. 7175-7195.

[23] S. Y. Sawant and M. H. Cho, *Facile electrochemical assisted synthesis of ZnO/graphene nanosheets with enhanced photocatalytic activity.* RSC advances, 2015. **5**(118): p. 97788-97797.

[24] P. Hu, X. Liang, M. Yaseen, X. Sun, Z. Tong, Z. Zhao, and Z. J. C. E. J. Zhao, *Preparation of highly-hydrophobic novel N-coordinated UiO-66 (Zr) with dopamine via fast mechano-chemical method for (CHO-/Cl-)-VOCs competitive adsorption in humid environment.* 2018. **332**: p. 608-618.

[25] N. S. M. Yusof and M. Ashokkumar, *Sonochemical synthesis of gold nanoparticles by using high intensity focused ultrasound.* ChemPhysChem, 2015. **16**(4): p. 775-781.

[26] R. Kumar, V. B. Kumar, and A. Gedanken, *Sonochemical synthesis of carbon dots, mechanism, effect of parameters, and catalytic, energy, biomedical and tissue engineering applications.* Ultrasonics Sonochemistry, 2020. **64**: p. 1-16.

[27] M. Senthil Pandian and P. Ramasamy, *Conventional slow evaporation and Sankaranarayanan–Ramasamy (SR) method grown diglycine zinc chloride (DGZC) single crystal and its comparative study.* Journal of Crystal Growth, 2010. **312**(3): p. 413-419.

[28] C. Dey, T. Kundu, B. P. Biswal, A. Mallick, and R. Banerjee, *Crystalline metal-organic frameworks (MOFs): synthesis, structure and function.* Acta Crystallographica Section B: Structural Science, Crystal Engineering, 2014. **70**(1): p. 3-10.

[29] N. Stock and S. Biswas, *Synthesis of metal-organic frameworks (MOFs): routes to various MOF topologies, morphologies, and composites.* Chemical reviews, 2012. **112**(2): p. 933-969.

[30] P. Falcaro, R. Ricco, A. Yazdi, I. Imaz, S. Furukawa, D. Maspoch, R. Ameloot, J. D. Evans, and C. Doonan, *Application of metal and metal oxide nanoparticles@ MOFs.* Coordination Chemistry Reviews, 2016. **307**: p. 237-254.

[31] X. Yang, Q. Xu, and Design, *Bimetallic metal–organic frameworks for gas storage and separation.* Crystal Growth, 2017. **17**(4): p. 1450-1455.

[32] S. R. Ahrenholtz, C. C. Epley, and A. J. Morris, *Solvothermal preparation of an electrocatalytic metalloporphyrin MOF thin film and its redox hopping charge-transfer mechanism.* Journal of the American Chemical Society, 2014. **136**(6): p. 2464-2472.

[33] J. Liu, D. Zhu, C. Guo, A. Vasileff, and S. Z. Qiao, *Design strategies toward advanced MOF-derived electrocatalysts for energy-conversion reactions.* Advanced Energy Materials, 2017. **7**(23): p. 1-26.

[34] P.-Q. Liao, J.-Q. Shen, and J.-P. Zhang, *Metal–organic frameworks for electrocatalysis.* Coordination Chemistry Reviews, 2018. **373**: p. 22-48.

[35] S. Kempahanumakkagari, K. Vellingiri, A. Deep, E. E. Kwon, N. Bolan, and K.-H. Kim, *Metal–organic framework composites as electrocatalysts for electrochemical sensing applications.* Coordination Chemistry Reviews, 2018. **357**: p. 105-129.

[36] A. A. Bunaciu, E. G. UdriŞTioiu, and H. Y. Aboul-Enein, *X-ray diffraction: instrumentation and applications.* Critical reviews in analytical chemistry, 2015. **45**(4): p. 289-299.

[37] K. D. Vernon-Parry, *Scanning electron microscopy: an introduction.* III-Vs Review, 2000. **13**(4): p. 40-44.

[38] H. Leamy, *Charge collection scanning electron microscopy.* Journal of Applied Physics, 1982. **53**(6): p. 51-80.

[39] L. Dzene, *Synthesis of scleroglucan-smectite composite based on Porto Santo bentonite*. 2014, Université d'Ottawa/University of Ottawa. p. 1-129.

[40] D. J. Gardiner, *Introduction to Raman scattering*, in *Practical Raman Spectroscopy*. 1989, Springer. p. 1-12.

[41] X. He, X. Liu, B. Nie, and D. Song, *FTIR and Raman spectroscopy characterization of functional groups in various rank coals.* Fuel, 2017. **206**: p. 555-563.

[42] X. Yang, J. Xue, and L. Feng, *Pt nanoparticles anchored over Te nanorods as a novel and promising catalyst for methanol oxidation reaction.* Chemical Communications, 2019. **55**(75): p. 11247-11250.

[43] T. Radhakrishnan and N. Sandhyarani, *Pt-Ag nanostructured 3D architectures: A tunable catalyst for methanol oxidation reaction.* Electrochimica Acta, 2019. **298**: p. 835-843.

[44] B. Abida, L. Chirchi, S. Baranton, T. W. Napporn, H. Kochkar, J.-M. Léger, and A. J. A. C. B. E. Ghorbel, *Preparation and characterization of Pt/TiO2 nanotubes catalyst for methanol electro-oxidation.* 2011. **106**(3-4): p. 609-615.

[45] I. S. Pieta, A. Rathi, P. Pieta, R. Nowakowski, M. Hołdynski, M. Pisarek, A. Kaminska, M. B. Gawande, and R. Zboril, *Electrocatalytic methanol oxidation over Cu, Ni and*

bimetallic Cu-Ni nanoparticles supported on graphitic carbon nitride. Applied Catalysis B: Environmental, 2019. **244**: p. 272-283.

[46] T. Noor, S. Pervaiz, N. Iqbal, H. Nasir, N. Zaman, M. Sharif, and E. Pervaiz, *Nanocomposites of NiO/CuO Based MOF with rGO: An Efficient and Robust Electrocatalyst for Methanol Oxidation Reaction in DMFC.* Nanomaterials, 2020. **10**(8): p. 1-18.

[47] L. Yaqoob, T. Noor, N. Iqbal, H. Nasir, and N. Zaman, *Development of nickel-BTC-MOF-derived nanocomposites with rGO towards electrocatalytic oxidation of methanol and its product analysis.* Catalysts, 2019. **9**(10): p. 1-21.

[48] X. Shi, *Pt/Pt Alloy and Manganese Dioxides Based Oxygen Reduction Reaction Catalysts for Low-Temperature Fuel Cells*. 2019, Arizona State University.

[49] R. Mehek, N. Iqbal, T. Noor, H. Nasir, Y. Mehmood, and S. Ahmed, *Novel Co-MOF/graphene oxide electrocatalyst for methanol oxidation.* Electrochimica Acta, 2017. **255**: p. 195-204.

[50] Y. Li, L. Tang, and J. Li, *Preparation and electrochemical performance for methanol oxidation of Pt/graphene nanocomposites.* Electrochemistry Communications, 2009. **11**(4): p. 846-849.

[51] X. Ma, K. Qi, S. Wei, L. Zhang, and X. Cui, *In situ encapsulated nickel-copper nanoparticles in metal-organic frameworks for oxygen evolution reaction.* Journal of Alloys and Compounds, 2019. **770**: p. 236-242.

[52] Y. Huang, S. Zheng, X. Lin, L. Su, and Y. Guo, *Microwave synthesis and electrochemical performance of a PtPb alloy catalyst for methanol and formic acid oxidation.* Electrochimica Acta, 2012. **63**: p. 346-353.

[53] Z. K. Ghouri, N. A. Barakat, H. Y. Kim, M. Park, K. A. Khalil, M. H. El-Newehy, and S. S. Al-Deyab, *Nano-engineered ZnO/CeO2 dots@ CNFs for fuel cell application.* Arabian Journal of Chemistry, 2016. **9**(2): p. 219-228.

[54] M. S. Rahmanifar, H. Hesari, A. Noori, M. Y. Masoomi, A. Morsali, and M. F. Mousavi, *A dual Ni/Co-MOF-reduced graphene oxide nanocomposite as a high performance supercapacitor electrode material.* Electrochimica Acta, 2018. **275**: p. 76-86.

[55] S. Mahapatra and J. Datta, *Characterization of Pt-Pd/C electrocatalyst for methanol oxidation in alkaline medium.* International Journal of Electrochemistry, 2011. **2011**: p. 1-16.

[56] M. K. Jeon, H. Daimon, K. R. Lee, A. Nakahara, and S. I. Woo, *CO tolerant Pt/WC methanol electro-oxidation catalyst.* Electrochemistry Communications, 2007. **9**(11): p. 2692-2695.

[57] T. Noor, M. Ammad, N. Zaman, N. Iqbal, L. Yaqoob, and H. Nasir, *A highly efficient and stable copper BTC metal organic framework derived electrocatalyst for oxidation of methanol in DMFC application.* Catalysis Letters, 2019. **149**(12): p. 3312-3327.

[58] J. Lan, C. Li, T. Liu, and Q. Yuan, *One-step synthesis of porous PtNiCu trimetallic nanoalloy with enhanced electrocatalytic performance toward methanol oxidation.* Journal of Saudi Chemical Society, 2019. **23**(1): p. 43-51.

[59] H. Ramezanalizadeh and F. Manteghi, *Immobilization of mixed cobalt/nickel metal-organic framework on a magnetic BiFeO3: a highly efficient separable photocatalyst for degradation of water pollutions.* J Journal of Photochemistry Photobiology A: Chemistry, 2017. **346**: p. 89-104.

[60] I. Danaee, M. Jafarian, F. Forouzandeh, F. Gobal, and M. Mahjani, *Electrochemical impedance studies of methanol oxidation on GC/Ni and GC/NiCu electrode.* International Journal of Hydrogen Energy, 2009. **34**(2): p. 859-869.

[61] V. Radmilovic, H. Gasteiger, and P. Ross, *Structure and chemical composition of a supported Pt-Ru electrocatalyst for methanol oxidation.* Journal of Catalysis, 1995. **154**(1): p. 98-106.

[62] S. Sun, M. Huang, P. Wang, and M. Lu, *Controllable hydrothermal synthesis of Ni/Co MOF as hybrid advanced electrode materials for supercapacitor.* Journal of The Electrochemical Society, 2019. **166**(10): p. 1799-1805.

[63] W. S. Hummers Jr and R. E. Offeman, *Preparation of graphitic oxide.* Journal of the american chemical society, 1958. **80**(6): p. 1339-1339.

[64] D. C. Marcano, D. V. Kosynkin, J. M. Berlin, A. Sinitskii, Z. Sun, A. S. Slesarev, L. B. Alemany, W. Lu, and J. M. Tour, *Correction to improved synthesis of graphene oxide.* ACS nano, 2018. **12**(2): p. 4806-4814.

[65] M. Haneef, H. Saleem, and A. Habib, *Use of graphene nanosheets and barium titanate as fillers in PMMA for dielectric applications.* Synthetic Metals, 2017. **223**: p. 101-106.

[66] P. T. Kissinger and W. R. Heineman, *Cyclic voltammetry.* Journal of Chemical Education, 1983. **60**(9): p. 702-706.

[67] A. Lasia, *Electrochemical impedance spectroscopy and its applications*, in *Modern aspects of electrochemistry*. 2002, Springer. p. 143-248.

[68] T. Gueshi, K. Tokuda, and H. Matsuda, *Voltammetry at partially covered electrodes: Part I. Chronopotentiometry and chronoamperometry at model electrodes.* Journal of Electroanalytical Chemistry and Interfacial Electrochemistry, 1978. **89**(2): p. 247-260.

[69] N. Sharma, V. Sharma, Y. Jain, M. Kumari, R. Gupta, S. Sharma, and K. Sachdev. *Synthesis and characterization of graphene oxide (GO) and reduced graphene oxide (rGO) for gas sensing application*. in *Macromolecular Symposia*. 2017. Wiley Online Library.

[70] V. H. Nguyen, T. D. Nguyen, L. G. Bach, T. Hoang, Q. T. P. Bui, L. D. Tran, C. V. Nguyen, D.-V. N. Vo, and S. T. Do, *Effective photocatalytic activity of mixed Ni/Fe-Base metal-organic framework under a compact fluorescent daylight lamp.* Catalysts, 2018. **8**(11): p. 487-507.

[71] M. Fathy, A. Gomaa, F. A. Taher, M. M. El-Fass, and A. E.-H. B. Kashyout, *Optimizing the preparation parameters of GO and rGO for large-scale production.* Journal of Materials Science, 2016. **51**(12): p. 5664-5675.

[72] M. Mukoyoshi, H. Kobayashi, K. Kusada, M. Hayashi, T. Yamada, M. Maesato, J. M. Taylor, Y. Kubota, K. Kato, and M. Takata, *Hybrid materials of Ni NP@ MOF prepared by a simple synthetic method.* Chemical Communications, 2015. **51**(62): p. 12463-12466.

[73] N. Cao and Y. Zhang, *Study of reduced graphene oxide preparation by Hummers' method and related characterization.* Journal of Nanomaterials, 2015. **2015**: p. 1-5.

[74] M. B. Askari, A. Beheshti-Marnani, M. Seifi, S. M. Rozati, and P. Salarizadeh, *Fe3O4 at MoS2/RGO as an effective nano-electrocatalyst toward electrochemical hydrogen evolution reaction and methanol oxidation in two settings for fuel cell application.* Journal of Colloid and Interface Science, 2019. **537**: p. 186-196.

[75] Y.-H. Huang, F.-M. Wang, T.-T. Huang, J.-M. Chen, B.-J. Hwang, and J. Rick, *Micro-electrode linked cyclic voltammetry study reveals ultra-fast discharge and high ionic*

transfer behavior of LiFePO4. International Journal of Electrochemical Science, 2012. **7**: p. 1205-1213.

[76] K. Kakaei, M. D. Esrafili, and A. Ehsani, *Graphene and Anticorrosive Properties*, in *Interface science and technology*. 2019, Elsevier. p. 303-337.

[77] F. Seland, R. Tunold, and D. A. Harrington, *Impedance study of methanol oxidation on platinum electrodes.* Electrochimica Acta, 2006. **51**(18): p. 3827-3840.

[78] R. Ganesan, D. J. Ham, and J. S. Lee, *Platinized mesoporous tungsten carbide for electrochemical methanol oxidation.* Electrochemistry Communications, 2007. **9**(10): p. 2576-2579.

[79] P. Yang, X. Yuan, H. Hu, Y. Liu, H. Zheng, D. Yang, L. Chen, M. Cao, Y. Xu, and Y. Min, *Solvothermal synthesis of alloyed PtNi colloidal nanocrystal clusters (CNCs) with enhanced catalytic activity for methanol oxidation.* Advanced Functional Materials, 2018. **28**(1): p. 1704774.

[80] S. Rezaee and S. Shahrokhian, *Facile synthesis of petal-like NiCo/NiO-CoO/nanoporous carbon composite based on mixed-metallic MOFs and their application for electrocatalytic oxidation of methanol.* Applied Catalysis B: Environmental, 2019. **244**: p. 802-813.